

A Linearity-Preserving Finite Volume Scheme with a Diamond Stencil for the Simulation of Anisotropic and Highly Heterogeneous Diffusion Problems using Tetrahedral Meshes

Ricardo J. M. de Lira Filho^{a,*}, Sidicley R. dos Santos^a, Túlio de M. Cavalcante^a, Fernando R. L. Contreras^b, Paulo R. M. Lyra^a, Darlan K. E. de Carvalho^a

^aUniversidade Federal de Pernambuco, Av. da Arquitetura, s/n, CEP: 50670-901, Recife, PE, Brazil

^bUniversidade Federal de Pernambuco, Núcleo de Tecnologia, Centro Acadêmico do Agreste, (NT-CAA), Rodovia BR 104 KM 59 s/n: 55002-970, Caruaru, PE-Brazil

Abstract

In this paper, we propose a non-orthodox Multipoint Flux Approximation scheme with a “Diamond” stencil (MPFA-D) for the solution of the 3-D steady state diffusion equation. Following the work of GAO and WU [1], in our method, the auxiliary vertex unknowns are eliminated by a novel explicit interpolation that is flux conservative and is constructed under the Linearity-Preserving Criterion (LPC). The MPFA-D is able to reproduce piecewise linear solutions exactly on challenging heterogeneous and anisotropic media, even in cases with some severely distorted meshes. Furthermore, our new scheme presents second order accuracy for the scalar unknown and, at least, first order accuracy for fluxes, considering unstructured tetrahedral meshes and arbitrarily anisotropic diffusion tensors. In order to validate our numerical scheme, we perform different test cases, involving 3-D benchmarks on diffusion problems. We compare the performance with other schemes found in literature. We also compare our Linearity-Preserving Explicit Weight (LPEW) interpolation with other interpolations strategies to evaluate its robustness to handle anisotropic and heterogeneous, possibly discontinuous diffusion tensors. In general, our linear preserving MPFA-D method performs well, however it is not monotone, particularly for very distorted meshes and highly anisotropic diffusion tensors.

Keywords: 3-D Diffusion Problem; Heterogeneous and Anisotropic Media; Non-Orthodox MPFA Method; Diamond Stencil; Linearity-Preserving Interpolation

1. Introduction

In many engineering and science fields, the diffusion equation can be found representing various phenomena, such as heat and mass transfer, flow through porous media, etc. For instance, in the context of fluid flow in porous media modeling, the diffusion coefficient represents the permeability of the media, which is, in general, represented by an anisotropic and heterogeneous, possibly discontinuous, tensor. Among the many important properties of numerical methods, accuracy, cost-efficiency and allowing arbitrary diffusion tensors are key features [1]. Hence, classical finite volume schemes such as the Two Point Flux Approximation (TPFA) might not capture the essence of the flow phenomenon neither for unstructured meshes nor for anisotropic full diffusive tensors.

Throughout the years, many MPFA schemes were developed (e.g. MPFA-O, MPFA-L, MPFA-FPS), in which the flux reconstruction stencils are different [2, 3, 4]. These formulations were compared and tested by many authors in 2-D and 3-D [1, 5, 6, 7, 8, 9]. Furthermore, it is often observed that many of these numerical methods seek to reproduce piecewise linear solutions exactly. Even though this requirement is not a necessary

*Corresponding author

Email address: r.liraf@gmail.com (Ricardo J. M. de Lira Filho)

or sufficient condition for convergence, many authors affirm that linearity-preserving schemes show enhanced accuracy even on highly skewed meshes [1, 10, 11, 12]. Moreover, in the presence of high-anisotropy ratios, even the more robust linear methods may be conditionally convergent and/or violate the discrete maximum principle (DMP), producing non-monotone solutions with spurious oscillations in the scalar field [5, 13, 14]. In the simulation of fluid flow through porous media, for instance, a spurious oscillating pressure field can generate fictitious gas in regions of the reservoir where the pressure falls erroneously below the bubble point, and these pressure fields are associated with non-physical Darcy velocities/fluxes [5].

Gao and Wu originally proposed the MPFA-D, which is both cell centered and vertex centered, for 2-D general and possibly non-conforming meshes [1]. Their method was tested [7, 15] on several 2-D benchmarks, found in [6]. In their scheme, the vertices variables are treated as intermediate unknowns. These unknown variables are expressed as a linear combination (or weighted combination) of the neighboring cell-centered unknowns. One of the main features of the proposed interpolations, LPEW1 and LPEW2, is the fact that they are constructed based on a flux conservative approach, which is desired in the case of mass conservation law methods. These interpolation methods were extensively explored in different contexts and methods, including non-linear monotone finite volumes [5, 7, 16, 17, 18].

There are many different methods for the vertex interpolation, easily found in the literature [1, 5]. Most of these methods, however, are only appropriate for isotropic media, thus facing problems in the presence of discontinuity. This means that the presence of moving discontinuities (such as saturation fronts) or skewed volumes in the domain will induce the interpolation method to fail or diminish the method's performance. Queiroz *et al.* [5] explored different interpolation methods with a non-linear finite volume scheme. They concluded that linear or inverse distance weighting interpolations (IDW) are not able to reproduce piecewise linear solutions exactly, i.e., it is not linear-preserving for general discontinuous diffusion tensors. Other similar MPFA schemes are found in the literature, however, not only are they complex formulations but also involve a great deal of computational cost, since the vertex expressions are not given explicitly, and therefore they are evaluated by solving certain local linear systems which might prove to be a difficult problem in certain cases [19].

Most of the development of these methods focus on 2-D domains. Several authors have explored and developed numerical schemes for 3-D domains, which are far more representative of different phenomena [2, 3, 20, 21, 22]. Eymard *et al.* [8] proposed a new set of benchmark tests for 3-D general diffusion schemes in 2011, given the much larger size of the linear systems that arise with these problems and the higher complexity compared to 2-D cases. Therefore, one common issue associated with 3-D domains is the fact that computational costs play an important role on the general performance for many of the 3-D methods. It is also important the ability to deal with unstructured meshes, as well as different types of geometries. Recent works based on the Mimetic Finite Difference (MFD), Lipnikov *et al.* [23], the Hybrid Finite Volume (HFV), Eymard *et al.* [24], and the Mixed Finite Volume Method (MFV), Droniou and Eymard [25], are among many important 3-D numerical schemes developed for diffusion problems.

The Discrete Duality Finite Volume scheme (DDFV) was proposed by Andreinov *et al.* [26]. This scheme consists of two systems, one for the (primary) cell centered and the other for the dual cells (vertex centred), which are fully coupled. Hermeline [27] further extended the DDFV. In this work, an indirect dual mesh is used in order to yield symmetric positive definite matrices. The indirect dual mesh is better for the 3-D framework and it provides a more accurate approximation of the gradient of the solution [27]. The “Diamond” stencil approach was studied by many authors [28, 29, 30, 31], mostly for 2-D domains. Lai *et al.* [19] proposed a 3-D approach in their monotone finite volume scheme that gives an explicit interpolation for the cell-vertex unknowns. It is a cell-centered scheme, and has an explicit expression for the normal fluxes on the cell faces, which makes the scheme different from above mentioned authors. However, this method does not possess second order accuracy for the scalar variable.

There is a great challenge in extending some 2-D methods for 3-D domains. Devising interpolation methods such as in [1] becomes a difficult task mainly due to the complexity associated to three-dimensional domains [32, 33]. For instance, some of the geometric features of the mesh elements might impose local ill conditioned problems, and therefore, some special treatment must be taken into account [34]. Yang and Gao [35] published a new interpolation method that satisfies the linearity-preserving criterion and is easily extended to 3-D domains. They have tested their method against several benchmark cases and have

obtained remarkable results.

In this work, we propose an extension of the MPFA-D for 3-D domains. This scheme is only cell centered for solving highly anisotropic and heterogeneous diffusive problems and an interpolation is constructed under the Linearity-Preserving Criterion (LPC) for eliminating the vertex auxiliary variables. Therefore, the vertex unknowns are replaced in the unique flux expression by a linear combination of the center unknowns, and the scheme becomes fully cell centered. The main novelty of our method lies in the construction of a flux conservative interpolation that outperforms other interpolations found in the literature [31]. In this sense, our method is a first of its kind for 3-D meshes. We call this interpolation “Linearity-Preserving Explicit Weight” (LPEW3) for its similarity with the interpolation strategies proposed by [1].

Since both the scheme formulation and the LPEW3 interpolation method satisfy the LPC, we are able to reproduce piecewise linear solutions exactly. We tested our method against benchmark diffusion problems on tetrahedral meshes, found in [6, 8, 36]. Its performance is compared against other formulations submitted to the benchmark data set. It is important to mention that our method is very robust for heterogeneous and general anisotropic diffusion tensors, even though it is not a monotone finite volume method and consequently it does not satisfy the Discrete Maximum Principle [2, 3, 36]. We also discuss the problems related to the interpolation method and monotonicity. To the day of this text, the method has not yet been tested on general polyhedral meshes although we do believe - and are investigating - that our interpolation method is capable to handle such cases.

The remaining of this paper is organized as follows. In Section 2, we briefly describe the mathematical model for the generalized diffusion problem. In Section 3, we present the detailed formulation of our MPFA-D scheme as well as the full description of our new interpolation method, LPEW3. Numerical experiments demonstrating the convergence rates and robustness of our scheme for heterogeneous and anisotropic media are presented in Section 4. Finally, we summarize the conclusions in Section 5.

2. Mathematical Formulation

The 3-D steady-state diffusion problem in heterogeneous and anisotropic media can be described by:

$$\nabla \cdot \vec{\mathcal{F}} = \mathcal{Q}(\vec{x}), \quad \text{with} \quad \vec{\mathcal{F}} = -\mathcal{K}(\vec{x})\nabla u \quad \text{in} \quad \vec{x} = (x, y, z) \in \Omega \subset \mathbb{R}^3. \quad (1)$$

In Eq. (1), $\vec{\mathcal{F}}$ represents a diffusive flux, such as in Fourier’s Law for heat conduction [37], the Darcy’s Law for flow through porous media [38] or Fick’s Law for mass diffusion [39], u is the scalar or potential variable, $\mathcal{Q}(\vec{x})$ is the source term. The diffusion coefficient $\mathcal{K}(\vec{x})$ is, in general, a positive definite symmetric full tensor that can be written, in Cartesian coordinates, as:

$$\mathcal{K}(\vec{x}) = \begin{pmatrix} \kappa_{xx} & \kappa_{xy} & \kappa_{xz} \\ \kappa_{yx} & \kappa_{yy} & \kappa_{yz} \\ \kappa_{zx} & \kappa_{zy} & \kappa_{zz} \end{pmatrix}. \quad (2)$$

Appropriate boundary conditions for the problem defined by Eq. (1), are given by:

$$\begin{aligned} u &= g_D && \text{on } \Gamma_D, \\ \vec{\mathcal{F}} \cdot \vec{n} &= g_N && \text{on } \Gamma_N, \end{aligned} \quad (3)$$

where the domain boundary $\partial\Omega = \Gamma_D \cup \Gamma_N$, and Γ_D and Γ_N represent the boundaries where Dirichlet and Neumann boundary conditions are imposed, and \vec{n} is the unitary outward normal vector.

3. Numerical Formulation

In this section, prior to the introduction of the 3-D formulation of the MPFA-D method, we first describe the gradient construction under the LPC. We also derive the unique flux expression for the MPFA-D scheme and introduce the LPEW3 interpolation method.

3.1. Construction of the gradient under the Linearity-Preserving Criterion

As described in Figure 1a, \mathcal{T}_{HIJK} is a generic control volume, with centroid \hat{R} and vertices I, J, K and H . The gradient, described in Eq. (1), for the scalar variable u is approximated on a sub-volume such as $\mathcal{T}_{\hat{R}IJK}$, shown in Figure 1b, formed by the I, J, K and the cell center \hat{R} , with height $h_{\hat{R}}$. In this region, we define normal area vectors pointing outward the faces of \mathcal{T}_{RIJK} such that:

$$\vec{N} = S \vec{n}, \quad (4)$$

where S is the area of the face and \vec{n} represents the unity outward face vector pointing outwards the control volume.

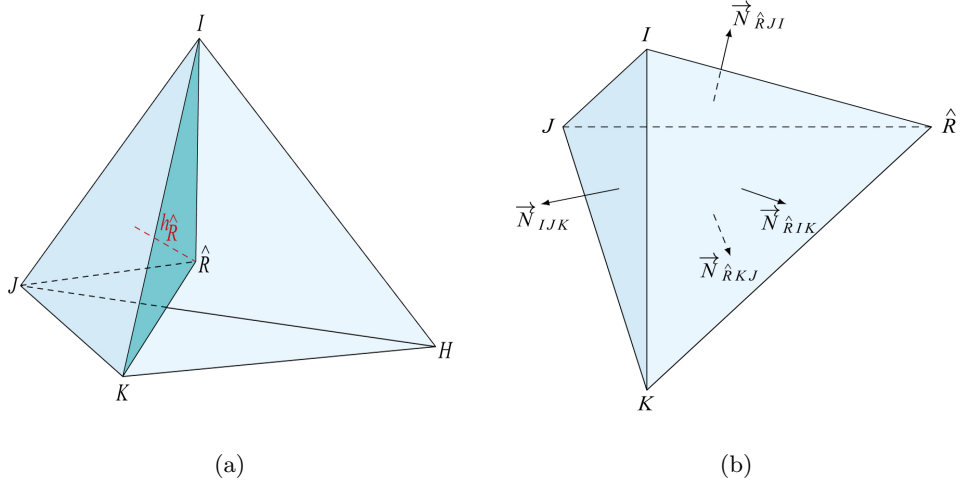


Figure 1: A control volume with center in \hat{R} and height $h_{\hat{R}}$ (1a). The inner region (1b) shows the normal area vectors for the gradient recovery.

Thus, we can define the gradient approximation, that satisfies the Linearity-Preserving Criterion (LPC), for \mathcal{T}_{RIJK} that can be written, as:

$$\begin{pmatrix} u_I - u_{\hat{R}} \\ u_K - u_{\hat{R}} \\ u_J - u_{\hat{R}} \end{pmatrix} \approx \begin{pmatrix} \vec{R}I^T \\ \vec{R}K^T \\ \vec{R}J^T \end{pmatrix} \nabla u_{\hat{R}} = \mathbf{X} \nabla u_{\hat{R}}, \quad (5)$$

and then:

$$\nabla u_{\hat{R}} \approx \mathbf{X}^{-1} \begin{pmatrix} u_I - u_{\hat{R}} \\ u_K - u_{\hat{R}} \\ u_J - u_{\hat{R}} \end{pmatrix}, \quad (6)$$

where \mathbf{X} is a 3×3 matrix formed by the transposed vectors $\vec{R}I$, $\vec{R}K$ and $\vec{R}J$, formed by the vertices $I = (\hat{I}_x, \hat{I}_y, \hat{I}_z)$, $J = (\hat{J}_x, \hat{J}_y, \hat{J}_z)$ and $K = (\hat{K}_x, \hat{K}_y, \hat{K}_z)$, and originated from $\hat{R} = (\hat{R}_x, \hat{R}_y, \hat{R}_z)$:

$$\mathbf{X} = \begin{bmatrix} \hat{I}_x - \hat{R}_x & \hat{I}_y - \hat{R}_y & \hat{I}_z - \hat{R}_z \\ \hat{K}_x - \hat{R}_x & \hat{K}_y - \hat{R}_y & \hat{K}_z - \hat{R}_z \\ \hat{J}_x - \hat{R}_x & \hat{J}_y - \hat{R}_y & \hat{J}_z - \hat{R}_z \end{bmatrix}. \quad (7)$$

The inverse of \mathbf{X} is given by:

$$\mathbf{X}^{-1} = \frac{1}{\det \mathbf{X}} \text{adj} \mathbf{X}, \quad (8)$$

where $\text{adj} \mathbf{X}$ represents the adjunct matrix to \mathbf{X} and the determinant, $\det \mathbf{X}$, is given by the triple product property of the vectors \vec{IR} , \vec{JR} and \vec{KR} which yields six times the volume of the tetrahedron $V_{\hat{R}}$. That is:

$$\det \mathbf{X} = \vec{RI} \cdot (\vec{RK} \times \vec{RJ}) = -6V_{\hat{R}}. \quad (9)$$

Therefore, Eq. (8) can be rearranged to yield:

$$\nabla u_{\hat{R}} \approx \frac{1}{6V_{\hat{R}}} \begin{bmatrix} \left| \begin{array}{cc} \hat{K}_y - \hat{R}_y & \hat{K}_z - \hat{R}_z \\ \hat{J}_y - \hat{R}_y & \hat{J}_z - \hat{R}_z \end{array} \right| & \left| \begin{array}{cc} \hat{K}_z - \hat{R}_z & \hat{K}_y - \hat{R}_y \\ \hat{I}_z - \hat{R}_z & \hat{I}_y - \hat{R}_y \end{array} \right| & \left| \begin{array}{cc} \hat{J}_y - \hat{R}_y & \hat{J}_z - \hat{R}_z \\ \hat{I}_y - \hat{R}_y & \hat{I}_z - \hat{R}_z \end{array} \right| \\ \left| \begin{array}{cc} \hat{K}_z - \hat{R}_z & \hat{K}_x - \hat{R}_x \\ \hat{J}_z - \hat{R}_z & \hat{J}_x - \hat{R}_x \end{array} \right| & \left| \begin{array}{cc} \hat{K}_x - \hat{R}_x & \hat{K}_z - \hat{R}_z \\ \hat{I}_x - \hat{R}_x & \hat{I}_z - \hat{R}_z \end{array} \right| & \left| \begin{array}{cc} \hat{J}_z - \hat{R}_z & \hat{J}_x - \hat{R}_x \\ \hat{I}_z - \hat{R}_z & \hat{I}_x - \hat{R}_x \end{array} \right| \\ \left| \begin{array}{cc} \hat{K}_x - \hat{R}_x & \hat{K}_y - \hat{R}_y \\ \hat{J}_x - \hat{R}_x & \hat{J}_y - \hat{R}_y \end{array} \right| & \left| \begin{array}{cc} \hat{K}_y - \hat{R}_y & \hat{K}_x - \hat{R}_x \\ \hat{I}_y - \hat{R}_y & \hat{I}_x - \hat{R}_x \end{array} \right| & \left| \begin{array}{cc} \hat{J}_x - \hat{R}_x & \hat{J}_y - \hat{R}_y \\ \hat{I}_x - \hat{R}_x & \hat{I}_y - \hat{R}_y \end{array} \right| \end{bmatrix} \begin{pmatrix} u_I - u_{\hat{R}} \\ u_K - u_{\hat{R}} \\ u_J - u_{\hat{R}} \end{pmatrix}, \quad (10)$$

or:

$$\nabla u_{\hat{R}} \approx \frac{1}{6V_{\hat{R}}} \begin{bmatrix} (u_I - u_{\hat{R}}) \left(\left| \begin{array}{cc} \hat{K}_y - \hat{R}_y & \hat{K}_z - \hat{R}_z \\ \hat{J}_y - \hat{R}_y & \hat{J}_z - \hat{R}_z \end{array} \right| \left| \begin{array}{cc} \hat{K}_z - \hat{R}_z & \hat{K}_y - \hat{R}_y \\ \hat{I}_z - \hat{R}_z & \hat{I}_y - \hat{R}_y \end{array} \right| \left| \begin{array}{cc} \hat{J}_y - \hat{R}_y & \hat{J}_z - \hat{R}_z \\ \hat{I}_y - \hat{R}_y & \hat{I}_z - \hat{R}_z \end{array} \right| \right) \\ + (u_K - u_{\hat{R}}) \left(\left| \begin{array}{cc} \hat{K}_z - \hat{R}_z & \hat{K}_x - \hat{R}_x \\ \hat{J}_z - \hat{R}_z & \hat{J}_x - \hat{R}_x \end{array} \right| \left| \begin{array}{cc} \hat{K}_x - \hat{R}_x & \hat{K}_z - \hat{R}_z \\ \hat{I}_x - \hat{R}_x & \hat{I}_z - \hat{R}_z \end{array} \right| \left| \begin{array}{cc} \hat{R}_z - \hat{J}_z & \hat{J}_x - \hat{R}_x \\ \hat{I}_z - \hat{R}_z & \hat{I}_x - \hat{R}_x \end{array} \right| \right) \\ + (u_J - u_{\hat{R}}) \left(\left| \begin{array}{cc} \hat{K}_x - \hat{R}_x & \hat{K}_y - \hat{R}_y \\ \hat{J}_x - \hat{R}_x & \hat{J}_y - \hat{R}_y \end{array} \right| \left| \begin{array}{cc} \hat{K}_y - \hat{R}_y & \hat{K}_x - \hat{R}_x \\ \hat{I}_y - \hat{R}_y & \hat{I}_x - \hat{R}_x \end{array} \right| \left| \begin{array}{cc} \hat{J}_x - \hat{R}_x & \hat{J}_y - \hat{R}_y \\ \hat{I}_x - \hat{R}_x & \hat{I}_y - \hat{R}_y \end{array} \right| \right) \end{bmatrix}. \quad (11)$$

Note that in eq. (11), the products between the potential differences of the scalar variable u by the 2×2 determinant factors yield a normal vector outward to one specific side of the tetrahedron:

$$\nabla u_{\hat{R}} \approx \frac{1}{3V_{\hat{R}}} \left[(u_I - u_{\hat{R}}) \vec{N}_{\hat{R}KJ} + (u_K - u_{\hat{R}}) \vec{N}_{\hat{R}JI} + (u_J - u_{\hat{R}}) \vec{N}_{\hat{R}IK} \right]. \quad (12)$$

3.2. Gradient Construction for the MPFA-D

Using the Gauss theorem [40], we have that:

$$\vec{N}_{\hat{R}IK} = -\vec{N}_{\hat{R}KJ} - \vec{N}_{\hat{R}JI} - \vec{N}_{IJK}. \quad (13)$$

Therefore, substituting eq. (13) in eq. (12), we have:

$$\nabla u_{\hat{R}} \approx \frac{1}{3V_{\hat{R}}} \left[(u_I - u_{\hat{R}}) \vec{N}_{\hat{R}KJ} + (u_K - u_{\hat{R}}) \vec{N}_{\hat{R}JI} + (u_J - u_{\hat{R}}) \left(-\vec{N}_{\hat{R}KJ} - \vec{N}_{\hat{R}JI} - \vec{N}_{IJK} \right) \right], \quad (14)$$

or:

$$\nabla u_{\hat{R}} \approx \frac{1}{3V_{\hat{R}}} \left[(u_I - u_J) \vec{N}_{\hat{R}KJ} + (u_K - u_J) \vec{N}_{\hat{R}JI} + (u_R - u_J) \vec{N}_{IJK} \right]. \quad (15)$$

$\vec{N}_{\hat{R}KJ}$ and $\vec{N}_{\hat{R}JI}$ can be replaced by, respectively:

$$2\vec{N}_{\hat{R}KJ} = \vec{JR} \times \vec{JK}, \quad (16)$$

$$2\vec{N}_{\hat{R}II} = \vec{JI} \times \vec{JR}. \quad (17)$$

Thus, eq. (15), yields:

$$\nabla u_{\hat{R}} \approx \frac{1}{6V_{\hat{R}}} \left[(u_I - u_J)(\vec{JR} \times \vec{JK}) + (u_K - u_J)(\vec{JI} \times \vec{JR}) + 2(u_{\hat{R}} - u_J)\vec{N}_{IJK} \right]. \quad (18)$$

Note that \vec{JR} can be rewritten as a combination of \vec{JI} , \vec{JK} and \vec{N}_{IJK} based on the quadruple product identity [41]. As long as the latter forms a non co-planar basis, we have the following identity:

$$\vec{JR} = m\vec{JI} + n\vec{JK} + w\vec{N}_{IJK}, \quad (19)$$

with:

$$m = \frac{\langle (\vec{JK} \times \vec{N}_{IJK}), \vec{JR} \rangle}{2|\vec{N}_{IJK}|^2}, \quad n = \frac{\langle (\vec{N}_{IJK} \times \vec{JI}), \vec{JR} \rangle}{2|\vec{N}_{IJK}|^2}, \quad w = \frac{h_{\hat{R}}}{|\vec{N}_{IJK}|}. \quad (20)$$

Performing the proper substitution of the expressions given in eq. (19) into eq. (18), we get:

$$\begin{aligned} \nabla u_{\hat{R}} \approx & \frac{1}{6V_{\hat{R}}} \left[(u_I - u_J) \left(\frac{\langle (\vec{JK} \times \vec{N}_{IJK}), \vec{JR} \rangle}{2|\vec{N}_{IJK}|^2} \vec{JI} \times \vec{JK} + \frac{h_{\hat{R}}}{|\vec{N}_{IJK}|} \vec{N}_{IJK} \times \vec{JK} \right) + \right. \\ & \left. (u_K - u_J) \left(\frac{\langle (\vec{N}_{IJK} \times \vec{JI}), \vec{JR} \rangle}{2|\vec{N}_{IJK}|^2} \vec{JI} \times \vec{JK} + \frac{h_{\hat{R}}}{|\vec{N}_{IJK}|} \vec{JI} \times \vec{N}_{IJK} \right) + 2(u_J - u_{\hat{R}})\vec{N}_{IJK} \right]. \end{aligned} \quad (21)$$

Eq. (21) similarly satisfies the relation with the area vector $-2\vec{N}_{IJK}$ and the vector product $\vec{JI} \times \vec{JK}$ such as in eq. (16). Also, the cross product $\vec{\tau}_{JK}$ is a vector defined in the face IJK , thus orthogonal to \vec{N}_{IJK} . Therefore, we call this tangent vector as $\vec{\tau}_{JK} = \vec{N}_{IJK} \times \vec{JK}$. Using that, we get:

$$\begin{aligned} \nabla u_{\hat{R}} \approx & \frac{1}{6V_{\hat{R}}} \left[(u_I - u_J) \left(- \frac{\langle \vec{\tau}_{JK}, \vec{JR} \rangle}{|\vec{N}_{IJK}|^2} \vec{N}_{IJK} + \frac{h_{\hat{R}}}{|\vec{N}_{IJK}|} \vec{\tau}_{JK} \right) + \right. \\ & \left. (u_J - u_K) \left(- \frac{\langle \vec{\tau}_{JI}, \vec{JR} \rangle}{|\vec{N}_{IJK}|^2} \vec{N}_{IJK} + \frac{h_{\hat{R}}}{|\vec{N}_{IJK}|} \vec{\tau}_{JI} \right) + 2(u_J - u_{\hat{R}}) \cdot \vec{N}_{IJK} \right]. \end{aligned} \quad (22)$$

3.3. The Unique Flux Expression

The diffusive flux given in eq. (1) can be approximated at the face IJK considering volume \hat{R} by replacing eq. (22) in the gradient expression, $\nabla u_{\hat{R}}$:

$$\begin{aligned} \vec{\mathcal{F}}_{\hat{R}} \cdot \vec{N}_{IJK} \approx & -\frac{\mathcal{K}_{\hat{R}}}{6V_{\hat{R}}} \left[(u_I - u_J) \left(- \frac{\langle \vec{\tau}_{JK}, \vec{JR} \rangle}{|\vec{N}_{IJK}|^2} \vec{N}_{IJK} + \frac{h_{\hat{R}}}{|\vec{N}_{IJK}|} \vec{\tau}_{JK} \right) + \right. \\ & \left. (u_J - u_K) \left(- \frac{\langle \vec{\tau}_{JI}, \vec{JR} \rangle}{|\vec{N}_{IJK}|^2} \vec{N}_{IJK} + \frac{h_{\hat{R}}}{|\vec{N}_{IJK}|} \vec{\tau}_{JI} \right) + 2(u_J - u_{\hat{R}}) \cdot \vec{N}_{IJK} \right] \vec{N}_{IJK}. \end{aligned} \quad (23)$$

Rearranging eq. (23), we have:

$$\begin{aligned} \vec{\mathcal{F}}_{\hat{R}} \cdot \vec{N}_{IJK} &\approx - \left[(u_I - u_J) \cdot \left(- \frac{\langle \vec{\tau}_{JK}, \vec{JR} \rangle}{|\vec{N}_{IJK}|^2} \vec{N}_{IJK}^T \cdot \frac{\mathcal{K}_{\hat{R}}}{6V_{\hat{R}}} \cdot \vec{N}_{IJK} + \frac{h_{\hat{R}}}{|\vec{N}_{IJK}|} \vec{N}_{IJK}^T \cdot \frac{\mathcal{K}_{\hat{R}}}{6V_{\hat{R}}} \vec{\tau}_{JK} \right) + \right. \\ &\quad \left. (u_J - u_K) \cdot \left(- \frac{\langle \vec{\tau}_{JI}, \vec{JR} \rangle}{|\vec{N}_{IJK}|^2} \vec{N}_{IJK}^T \cdot \frac{\mathcal{K}_{\hat{R}}}{6V_{\hat{R}}} \vec{N}_{IJK} + \frac{h_{\hat{R}}}{|\vec{N}_{IJK}|} \vec{N}_{IJK}^T \cdot \frac{\mathcal{K}_{\hat{R}}}{6V_{\hat{R}}} \vec{\tau}_{JK} \right) + 2(u_J - u_{\hat{R}}) \vec{N}_{IJK}^T \cdot \frac{\mathcal{K}_{\hat{R}}}{6V_{\hat{R}}} \cdot \vec{N}_{IJK} \right] \end{aligned} \quad (24)$$

Using eq. 9 and after some algebraic manipulation, we can rewrite the flux definition of eq (24) as:

$$\begin{aligned} \vec{\mathcal{F}}_{\hat{R}} \cdot \vec{N}_{IJK} &\approx - \left[(u_I - u_J) \left(- \frac{\langle \vec{\tau}_{JK}, \vec{JR} \rangle}{|\vec{N}_{IJK}|^2} \frac{K_{\hat{R}}^{(n)}}{h_{\hat{R}}} + \frac{h_{\hat{R}}}{|\vec{N}_{IJK}|} \frac{K_{\hat{R}}^{JK}}{h_{\hat{R}}} \right) + \right. \\ &\quad \left. (u_J - u_K) \left(- \frac{\langle \vec{\tau}_{JI}, \vec{JR} \rangle}{|\vec{N}_{IJK}|^2} \frac{K_{\hat{R}}^{(n)}}{h_{\hat{R}}} + \frac{h_{\hat{R}}}{|\vec{N}_{IJK}|} \frac{K_{\hat{R}}^{JI}}{h_{\hat{R}}} \right) + 2(u_J - u_{\hat{R}}) \frac{K_{\hat{R}}^{(n)}}{h_{\hat{R}}} \right], \end{aligned} \quad (25)$$

with:

$$K_{\hat{R}}^n = \left(\frac{\vec{N}_{IJK}^T \mathcal{K}_{\hat{R}} \cdot \vec{N}_{IJK}}{2 |\vec{N}_{IJK}|} \right), \quad K_{\hat{R}}^{JK} = \left(\frac{\vec{N}_{IJK}^T \mathcal{K}_{\hat{R}} \cdot \vec{\tau}_{JK}}{2 |\vec{N}_{IJK}|} \right), \quad K_{\hat{R}}^{JI} = \left(\frac{\vec{N}_{IJK}^T \mathcal{K}_{\hat{R}} \cdot \vec{\tau}_{JI}}{2 |\vec{N}_{IJK}|} \right). \quad (26)$$

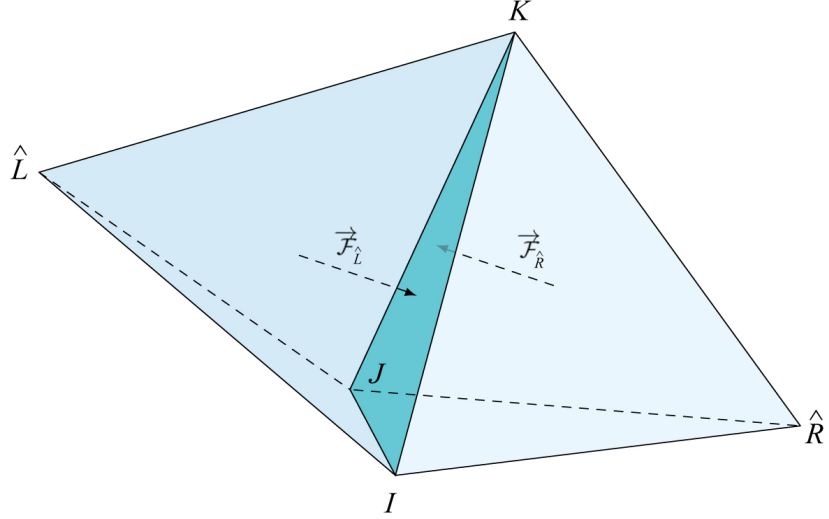


Figure 2: Two tetrahedra sharing face IJK for the calculation of the unique flux expression.

Eq. (25) can be modified by multiplying it by $\frac{h_{\hat{R}}}{K_{\hat{R}}^{(n)}}$:

$$\frac{h_{\hat{R}}}{K_{\hat{R}}^{(n)}} \vec{\mathcal{F}}_{\hat{R}} \cdot \vec{N}_{IJK} \approx - \left[(u_I - u_J) \cdot \left(- \frac{\langle \vec{\tau}_{JK}, \vec{JR} \rangle}{|\vec{N}_{IJK}|^2} + \frac{K_{\hat{R}}^{JK}}{K_{\hat{R}}^{(n)}} \right) + (u_J - u_K) \cdot \left(- \frac{\langle \vec{\tau}_{JI}, \vec{JR} \rangle}{|\vec{N}_{IJK}|^2} + \frac{K_{\hat{R}}^{JI}}{K_{\hat{R}}^{(n)}} \right) + 2(u_J - u_{\hat{R}}) \right]. \quad (27)$$

Note that similar a procedure can be done for the volume \hat{L} , adjacent to \hat{R} by the face IJK (see figure 2).

$$\frac{h_{\hat{L}}}{K_{\hat{L}}^{(n)}} \vec{\mathcal{F}}_{\hat{L}} \cdot (-\vec{N}_{IJK}) \approx - \left[(u_I - u_J) \cdot \left(- \frac{\langle \vec{\tau}_{JK}, \vec{LJ} \rangle}{|\vec{N}_{IJK}|^2} + \frac{K_{\hat{L}}^{JK}}{K_{\hat{L}}^{(n)}} \right) + (u_J - u_K) \cdot \left(- \frac{\langle \vec{\tau}_{JI}, \vec{LJ} \rangle}{|\vec{N}_{IJK}|^2} + \frac{K_{\hat{L}}^{JI}}{K_{\hat{L}}^{(n)}} \right) + 2(u_{\hat{L}} - u_J) \right]. \quad (28)$$

By using the continuity equation through face IJK, we have:

$$\vec{\mathcal{F}}_{\hat{R}} + \vec{\mathcal{F}}_{\hat{L}} = 0. \quad (29)$$

Replacing eq. (28) and (29) into eq. (27) we have the unique flux expression:

$$\vec{\mathcal{F}}_{\hat{R}} \cdot \vec{N}_{IJK} \approx -K_{eff}^{(n)} \left[2(u_{\hat{R}} - u_{\hat{L}}) - D_{JI}(u_I - u_J) - D_{JK}(u_K - u_J) \right], \quad (30)$$

where $K_{eff}^{(n)}$ is the harmonic average of projected diffusion tensor orthogonal to face IJK. D_{JI} and D_{JK} represent the cross diffusion term, or an averaged tangent projection of the diffusion tensor at IJK, as follows:

$$K_{eff}^{(n)} = \frac{K_{\hat{R}}^{(n)} K_{\hat{L}}^{(n)}}{K_{\hat{R}}^{(n)} h_{\hat{L}} + K_{\hat{L}}^{(n)} h_{\hat{R}}}, \quad (31)$$

$$D_{JI} = \frac{\langle \vec{\tau}_{JK}, \vec{LR} \rangle}{|\vec{N}_{IJK}|^2} - \frac{1}{|\vec{N}_{IJK}|} \left(\frac{K_{\hat{R}}^{JK}}{K_{\hat{R}}^{(n)}} h_{\hat{R}} + \frac{K_{\hat{L}}^{JK}}{K_{\hat{L}}^{(n)}} h_{\hat{L}} \right), \quad (32)$$

$$D_{JK} = \frac{\langle \vec{\tau}_{JI}, \vec{LR} \rangle}{|\vec{N}_{IJK}|^2} - \frac{1}{|\vec{N}_{IJK}|} \left(\frac{K_{\hat{R}}^{JI}}{K_{\hat{R}}^{(n)}} h_{\hat{R}} + \frac{K_{\hat{L}}^{JI}}{K_{\hat{L}}^{(n)}} h_{\hat{L}} \right). \quad (33)$$

3.4. Boundary Conditions

The flux at any face submitted to Dirichlet boundary conditions given by eq. (3), can be calculated using eq. (25), which by simplifying yields:

$$\vec{\mathcal{F}}_{\hat{R}} \approx - \left[2 \frac{K_{\hat{R}}^{(n)}}{h_{\hat{R}}} (u_{\hat{R}} - g_J^D) + D_{JI}(g_J^D - g_I^D) + D_{JK}(g_J^D - g_K^D) \right], \quad (34)$$

where g_I^D , g_J^D e g_K^D are prescribed values defined on the boundaries, with D_{JI} and D_{JK} :

$$D_{JI} = -\frac{\langle \vec{\tau}_{JK}, \vec{J}\hat{R} \rangle}{|\vec{N}_{IJK}|} \frac{K_{\hat{R}}^{(n)}}{h_{\hat{R}}} + K_{\hat{R}}^{JK}, \quad (35)$$

$$D_{JK} = -\frac{\langle \vec{\tau}_{JI}, \vec{J}\hat{R} \rangle}{|\vec{N}_{IJK}|} \frac{K_{\hat{R}}^{(n)}}{h_{\hat{R}}} + K_{\hat{R}}^{JI}. \quad (36)$$

Also, the flux at any face submitted to Neumann boundary conditions can be defined by:

$$\vec{\mathcal{F}}_{\hat{R}} \cdot \vec{N}_{IJK} = g_N. \quad (37)$$

3.5. Elimination of the vertex unknowns based on a flux conservative interpolation method: The LPEW3

In order to eliminate the auxiliary vertex unknowns to keep our flux approximation fully cell centered, we write the vertex variable as a linear combination of cell centered unknowns as:

$$u_Q = \sum_{\hat{k}=1}^{N_Q} \omega_{\hat{k}} u_{\hat{k}}, \quad (38)$$

with u_Q being the scalar property at the vertex Q . N_Q is the number of volumes surrounding Q , and $\omega_{\hat{k}}$ is the weight associated to each volume \hat{k} , where the scalar $u_{\hat{k}}$ is the finite volume value associated at its centroid (although this is not necessary).

3.5.1. Interpolation of the scalar variable for an inner vertex

Figure 3a shows the support region for the interpolation of u_Q , such that the collection of volumes surrounding the vertex Q (N_Q) is defined by all volumes that share the interpolated vertex. Auxiliary vertices at the boundary of the support region are represented in figure 3b for a single volume in N_Q . These auxiliary vertex, T_1 , T_2 and T_3 - will be explicit out of the expression in eq. (38). For that, we impose the mass conservation law in the region aforementioned. Thus, the flux from a generic volume \hat{k} outward the control volume at the face opposite to vertex Q , i.e. face $T_1 T_2 T_3$, is given by:

$$\vec{\mathcal{F}}_{\hat{k}} \cdot \vec{N}_Q^{\hat{k}} = \frac{\mathcal{K}_{\hat{k}}}{3V_{\hat{k}}} [(u_{T_1} - u_Q) \vec{N}_{T_3 T_2 Q} + (u_{T_2} - u_Q) \vec{N}_{T_1 T_3 Q} + (u_{T_3} - u_Q) \vec{N}_{T_2 T_1 Q}] \cdot \vec{N}_Q^{\hat{k}}, \quad (39)$$

and by the mass conservation law, the sum of all fluxes from the N_Q volumes is given by:

$$\sum_{\hat{k}=1}^{N_Q} \vec{\mathcal{F}}_{\hat{k}} \cdot \vec{N}_Q^{\hat{k}} = 0, \quad (40)$$

where $\vec{N}_Q^{\hat{k}}$ is the area vector of the face opposite to the vertex Q inside volume \hat{k} . Consider also that neighbor O_j is the volume that shares the face opposite to T_j (see figure 4). $\vec{N}_{T_j}^{\hat{k}}$ is the area vector defined by the face opposite to the vertex j .

In order to obtain an explicit expression for the flux in terms of cell centered unknowns, we impose flux continuity between \hat{k} and its neighbors as presented in Eq. (41):

$$\vec{\mathcal{F}}_{\hat{k}|O_1} \cdot \vec{N}_{T_j}^{\hat{k}} + \vec{\mathcal{F}}_{O_j|\hat{k}} \cdot (-\vec{N}_{T_j}^{\hat{k}}) = 0. \quad (41)$$

The flux from \hat{k} to O_1 is denoted by $\hat{k}|O_1$ and is given by:

$$\vec{\mathcal{F}}_{\hat{k}|O_1} \cdot \vec{N}_{T_1}^{\hat{k}} = -\frac{\mathcal{K}_{\hat{k}}}{3V_{\hat{k}|O_1}} [(u_{T_2} - u_Q) \vec{N}_{T_3 Q \hat{k}} + (u_{T_3} - u_Q) \vec{N}_{\hat{k} Q T_2} + (u_{\hat{k}} - u_Q) \vec{N}_{T_2 Q T_3}] \cdot \vec{N}_{T_1}^{\hat{k}}. \quad (42)$$

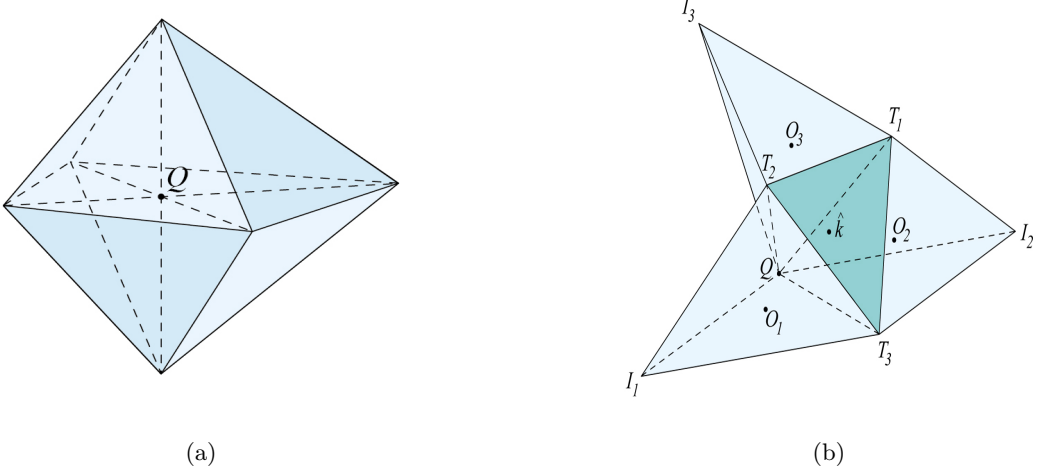


Figure 3: A generic vertex Q and the full interpolation support region (3a). Part of the support region for the interpolation vertex Q showing all the surrounding volumes that share a face with the volume \hat{k} (3b).

Analogously, flux from O_1 towards \hat{k} represented as $O_1|\hat{k}$ and is given by:

$$\vec{\mathcal{F}}_{O_1|\hat{k}} \cdot (-\vec{N}_{T_1}^{\hat{k}}) = \frac{\mathcal{K}_{O_1}}{3V_{O_1|\hat{k}}} \left[(u_{T_2} - u_Q) \vec{N}_{O_1 QT_3} + (u_{T_3} - u_Q) \vec{N}_{T_3 Q O_1} + (u_{O_j} - u_Q) \vec{N}_{T_3 Q T_2} \right] \cdot \vec{N}_{T_1}^{\hat{k}}. \quad (43)$$

Replacing eqs. (42) and (43) in eq. (41), we have:

$$\begin{aligned} & \left(\vec{N}_{T_1}^{\hat{k}} \cdot \frac{\mathcal{K}_{O_1}}{3V_{O_1|\hat{k}}} \vec{N}_{O_1 QT_3} - \vec{N}_{T_1}^{\hat{k}} \cdot \frac{\mathcal{K}_{\hat{k}}}{3V_{\hat{k}|O_1}} \vec{N}_{T_3 Q \hat{k}} \right) (u_{T_2} - u_Q) + \\ & \left(\vec{N}_{T_1}^{\hat{k}} \cdot \frac{\mathcal{K}_{O_1}}{3V_{O_1|\hat{k}}} \vec{N}_{T_3 Q O_1} - \vec{N}_{T_1}^{\hat{k}} \cdot \frac{\mathcal{K}_{\hat{k}}}{3V_{\hat{k}|O_1}} \vec{N}_{\hat{k} Q T_2} \right) (u_{T_3} - u_Q) + \\ & = \vec{N}_{T_1}^{\hat{k}} \cdot \frac{\mathcal{K}_{\hat{k}}}{3V_{\hat{k}|O_1}} \vec{N}_{T_1}^{\hat{k}} (u_{\hat{k}} - u_Q) + \vec{N}_{T_1}^{\hat{k}} \cdot \frac{\mathcal{K}_{O_1}}{3V_{O_1|\hat{k}}} \vec{N}_{T_1}^{\hat{k}} (u_{O_1} - u_Q) \end{aligned} \quad (44)$$

We can rewrite eq. (44) as:

$$(\xi_{O_1|\hat{k}}^{T_2} - \xi_{\hat{k}|O_1}^{T_2}) (u_{T_2} - u_Q) + (\xi_{O_1|\hat{k}}^{T_3} - \xi_{\hat{k}|O_1}^{T_3}) (u_{T_3} - u_Q) = \xi_{\hat{k}|O_1} (u_{\hat{k}} - u_Q) + \xi_{O_1|\hat{k}} (u_{O_1} - u_Q). \quad (45)$$

$\xi_{A|B}^{T_i}$ is defined by the expression:

$$\xi_{A|B}^{T_i} = \vec{N}_{T_i}^{\hat{k}^T} \frac{\mathcal{K}_A}{3V_{A|B}} \vec{N}_{T_i}^{A|B}, \quad \xi_{A|B} = \vec{N}_{T_i}^{\hat{k}^T} \frac{\mathcal{K}_A}{3V_{A|B}} \vec{N}_{T_i}^{\hat{k}} \quad (46)$$

where $\vec{N}_{T_i}^A$ is defined within the support volume formed by AQT_iT_{i+1} . Also, A and B are defined such that:

$$A = \{\hat{k}, O_j\}, B = \{\hat{k}, O_j\}, \quad \text{with } A \neq B, \quad (47)$$

and $\vec{N}_{T_i}^{A|B}$ is one of the normal area vectors of the tetrahedron formed by the centroid of A and the face shared by A and B.

By defining:

$$\lambda_{A|B}^{T_i} = \xi_{A|B}^{T_i} - \xi_{B|A}^{T_i}, \quad (48)$$

and replacing that in the terms of eq. (45), we get:

$$\left(\lambda_{O_1|\hat{k}}^{T_2} \right) (u_{T_2} - u_Q) + \left(\lambda_{O_1|\hat{k}}^{T_3} \right) (u_{T_3} - u_Q) = \xi_{O_1|\hat{k}} (u_{O_1} - u_Q) + \xi_{\hat{k}|O_1} (u_{\hat{k}} - u_Q). \quad (49)$$

Performing a similar procedure from eqs. (42) to (49) for all O_j neighboring volumes to \hat{k} , we have:

$$\left(\lambda_{O_2|\hat{k}}^{T_1} \right) (u_{T_1} - u_Q) + \left(\lambda_{O_2|\hat{k}}^{T_3} \right) (u_{T_3} - u_Q) = \xi_{O_2|\hat{k}} (u_{O_2} - u_Q) + \xi_{\hat{k}|O_2} (u_{\hat{k}} - u_Q), \quad (50)$$

$$\left(\lambda_{O_3|\hat{k}}^{T_1} \right) (u_{T_1} - u_Q) + \left(\lambda_{O_3|\hat{k}}^{T_2} \right) (u_{T_2} - u_Q) = \xi_{O_3|\hat{k}} (u_{O_3} - u_Q) + \xi_{\hat{k}|O_3} (u_{\hat{k}} - u_Q). \quad (51)$$

Solving the system defined by equations (49) - (51) leads to:

$$\begin{bmatrix} (u_{T_1} - u_Q) \\ (u_{T_2} - u_Q) \\ (u_{T_3} - u_Q) \end{bmatrix} = \frac{1}{\sigma_{\hat{k}}} A \begin{pmatrix} \xi_{O_1|\hat{k}} (u_{O_1} - u_Q) \\ \xi_{O_2|\hat{k}} (u_{O_2} - u_Q) \\ \xi_{O_3|\hat{k}} (u_{O_3} - u_Q) \end{pmatrix} + \begin{bmatrix} \xi_{\hat{k}|O_1} \\ \xi_{\hat{k}|O_2} \\ \xi_{\hat{k}|O_3} \end{bmatrix} (u_{\hat{k}} - u_Q) \quad (52)$$

The matrix A and the scalar $\sigma_{\hat{k}}$ are given by, respectively:

$$A = \begin{bmatrix} -\lambda_{O_2|\hat{k}}^{T_3} \lambda_{O_3|\hat{k}}^{T_2} & \lambda_{O_1|\hat{k}}^{T_3} \lambda_{O_3|\hat{k}}^{T_2} & \lambda_{O_1|\hat{k}}^{T_2} \lambda_{O_2|\hat{k}}^{T_3} \\ \lambda_{O_2|\hat{k}}^{T_3} \lambda_{O_3|\hat{k}}^{T_1} & -\lambda_{O_1|\hat{k}}^{T_3} \lambda_{O_3|\hat{k}}^{T_1} & \lambda_{O_1|\hat{k}}^{T_3} \lambda_{O_2|\hat{k}}^{T_1} \\ \lambda_{O_2|\hat{k}}^{T_1} \lambda_{O_3|\hat{k}}^{T_2} & \lambda_{O_1|\hat{k}}^{T_2} \lambda_{O_3|\hat{k}}^{T_1} & -\lambda_{O_1|\hat{k}}^{T_2} \lambda_{O_2|\hat{k}}^{T_1} \end{bmatrix}, \quad (53)$$

$$\sigma_{\hat{k}} = \lambda_{O_1|\hat{k}}^{T_2} \lambda_{O_2|\hat{k}}^{T_3} \lambda_{O_3|\hat{k}}^{T_1} + \lambda_{O_1|\hat{k}}^{T_3} \lambda_{O_2|\hat{k}}^{T_1} \lambda_{O_3|\hat{k}}^{T_2}. \quad (54)$$

Therefore, by replacing eq. (52) in eq. (39), we get:

$$\vec{\mathcal{F}}_{\hat{k}} \cdot \vec{N}_{Q|O_j}^{\hat{k}} = - \begin{bmatrix} \eta_{\hat{k}|O_1} & \eta_{\hat{k}|O_2} & \eta_{\hat{k}|O_3} \end{bmatrix} \frac{A}{\sigma_{\hat{k}}} \begin{pmatrix} \xi_{O_1|\hat{k}} (u_{O_1} - u_Q) \\ \xi_{O_2|\hat{k}} (u_{O_2} - u_Q) \\ \xi_{O_3|\hat{k}} (u_{O_3} - u_Q) \end{pmatrix} + \begin{bmatrix} \xi_{\hat{k}|O_1} \\ \xi_{\hat{k}|O_2} \\ \xi_{\hat{k}|O_3} \end{bmatrix} (u_{\hat{k}} - u_Q). \quad (55)$$

The sum of fluxes through all \hat{k} volumes, as in eq. (40) gives:

$$\sum_{\hat{k}=1}^{N_Q} \begin{bmatrix} \eta_{\hat{k}|O_1} & \eta_{\hat{k}|O_2} & \eta_{\hat{k}|O_3} \end{bmatrix} \frac{A}{\sigma_{\hat{k}}} \begin{pmatrix} \xi_{O_1|\hat{k}} (u_{O_1} - u_Q) \\ \xi_{O_2|\hat{k}} (u_{O_2} - u_Q) \\ \xi_{O_3|\hat{k}} (u_{O_3} - u_Q) \end{pmatrix} + \begin{bmatrix} \xi_{\hat{k}|O_1} \\ \xi_{\hat{k}|O_2} \\ \xi_{\hat{k}|O_3} \end{bmatrix} (u_{\hat{k}} - u_Q) = 0. \quad (56)$$

Note that $\eta_{Q|O_j}$ (similar to $\xi_{A|B}^{T_i}$) is defined by the expression:

$$\eta_{\hat{k}|O_j} = \vec{N}_Q^{k^T} \frac{\mathcal{K}_{\hat{k}}}{3V_{\hat{k}}} \vec{N}_{T_j}^{\hat{k}}. \quad (57)$$

Note that the difference $(u_{\hat{k}} - u_Q)$ will not only be part of the expression in eq. (56). The previous procedure in eqs (49) to (56) is applied to all O_j volumes, and therefore, the $(u_{\hat{k}} - u_Q)$ expressions should

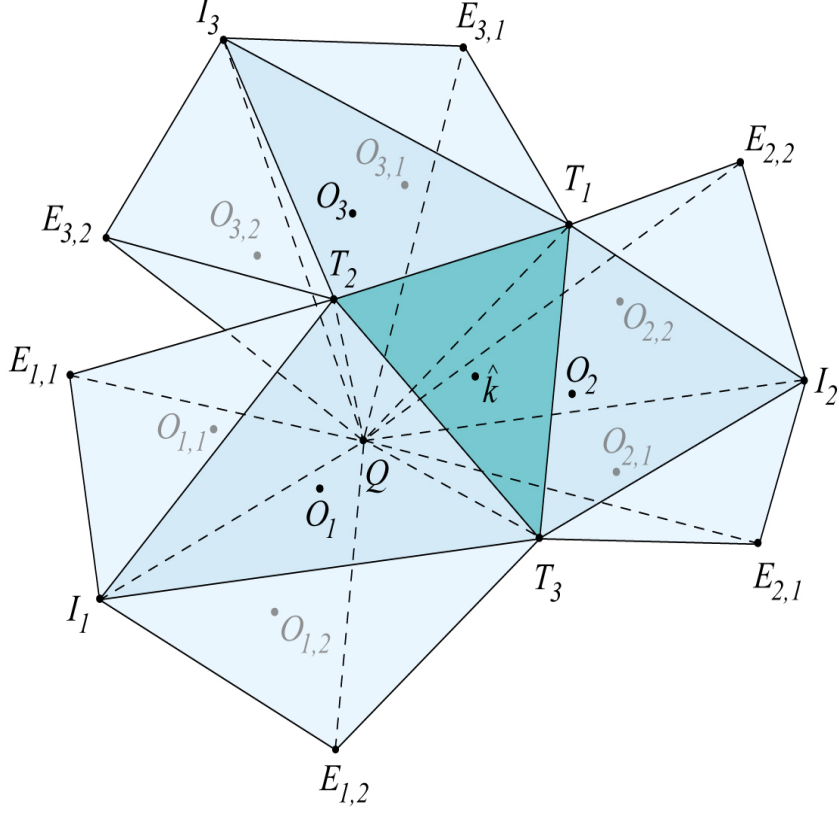


Figure 4: Adjacent volumes involved in the calculation of the flux through volume \hat{k} .

appear three more times, apart from appearing in eq (56). This is because \hat{k} plays the role of adjacent neighbor for each O_j volume. Then, we can rearrange eq. (56) to group only \hat{k} dependent terms, as:

$$\begin{aligned} \phi_{O_j|\hat{k}} &= \frac{\lambda_{O_{j,1}|O_j}^{T_{j+1}} \lambda_{O_{j,2}|O_j}^{T_{j+2}}}{\sigma_{O_j}} \eta_{O_j|\hat{k}} \xi_{\hat{k}|O_j}, & \phi_{\hat{k}|O_j} &= \frac{\lambda_{O_{j+1}|\hat{k}}^{T_{j+2}} \lambda_{O_{j+2}|\hat{k}}^{T_{j+1}}}{\sigma_{\hat{k}}} \eta_{\hat{k}|O_j} \xi_{\hat{k}|O_j} \\ \Psi_{O_j|O_{j,i}} &= \frac{\lambda_{O_{j,i}|O_j}^{T_{j+i}} \lambda_{O_{j,i+1}|O_j}^{T_j}}{\sigma_{O_j}} \eta_{O_j|O_{j,i}} \xi_{\hat{k}|O_j}, & \Psi_{O_j|O_i} &= \frac{\lambda_{O_i|\hat{k}}^{T_{2(j+i)}} \lambda_{O_{i+1}|\hat{k}}^{T_j}}{\sigma_{\hat{k}}} \eta_{\hat{k}|O_i} \xi_{\hat{k}|O_j} \end{aligned} \quad (58)$$

and then, eq. (56) can be written as:

$$\sum_{\hat{k}=1}^{N_Q} (\zeta_{\hat{k}} - \delta_{\hat{k}}) (u_{\hat{k}} - u_Q) = 0, \quad (59)$$

where:

$$\zeta_{\hat{k}} = \sum_{j=1}^3 \sum_{i=1}^2 \Psi_{O_j|O_{j,i}} + \sum_{j=1, i=1, j \neq i}^3 \Psi_{O_j|O_i}, \quad \delta_{\hat{k}} = \sum_{j=1}^3 \phi_{O_j|\hat{k}} + \sum_{j=1}^3 \phi_{\hat{k}|O_j}, \quad (60)$$

then, eq. (38) is written, as:

$$u_Q = \frac{\sum_{\hat{k}=1}^{N_Q} (\zeta_{\hat{k}} - \delta_{\hat{k}}) u_{\hat{k}}}{\sum_{\hat{k}=1}^{N_Q} (\zeta_{\hat{k}} - \delta_{\hat{k}})}, \quad \omega_{\hat{k}} = \frac{(\zeta_{\hat{k}} - \delta_{\hat{k}})}{\sum_{\hat{k}=1}^{N_Q} (\zeta_{\hat{k}} - \delta_{\hat{k}})}. \quad (61)$$

3.5.2. Interpolation of the scalar variable for a boundary vertex

If a vertex is located at the boundary with prescribed value for the scalar variable (Dirichlet boundary condition), then no interpolation is needed. On the other hand, if the flux is prescribed at the boundary (Neumann boundary condition), then the unknown value at the vertex must be interpolated. The support region for the interpolation will be composed of two different types of volumes: volumes that just have a node or edge in the boundary, denoted by \hat{k} , and volumes \hat{k}_N containing at least one of its faces within the boundary Γ_N of the domain.

Thus, similar to eq. (40) the total flux on the control volume surrounding any vertex $Q \in \Gamma_N$ is given by:

$$\sum_{\hat{k}} \vec{\mathcal{F}}_{\hat{k}} \cdot \vec{N}_{\hat{k}} + \sum_{\hat{k}_N} \left[\vec{\mathcal{F}}_{\hat{k}_N} \cdot \vec{N}_{\hat{k}_N} + \sum_{r_N} \left(g_{\hat{k}_N}^{r_N} S_{\hat{k}_N, r_N} \right) \right] = 0. \quad (62)$$

where $g_{\hat{k}_N}^{r_N}$ is the prescribed flux through the face r_N of control volume \hat{k}_N and $S_{\hat{k}_N, r_N}$ is the area of r_N .

Following similar procedure adopted in the previous section, we must now write the flux expressions for volumes \hat{k} and \hat{k}_N as an expression of volume centers only. For inner volumes, \hat{k} , the flux expression is identical to (59). Differently, treatment of flux through \hat{k}_N will consider continuity through the Neumann boundaries as well. Therefore, in these cases, eq. (41) will be written as:

$$\vec{\mathcal{F}}_{\hat{k}|r_N} \cdot \vec{N}_{T_j} = g_N^{r_N} |S_{\hat{k}, g_N, r_N}|. \quad (63)$$

Suppose that $r_N = 2$ and $r_N \in \Gamma_N$. Then the volume \hat{k}_N will have only two neighbors: O_1 and O_2 . The continuity flux from \hat{k}_N towards these volumes and also the boundary mentioned is given by:

$$\begin{aligned} \lambda_{O_1|\hat{k}_N}^{T_2} (u_{T_2} - u_Q) + \lambda_{O_1|\hat{k}_N}^{T_3} (u_{T_3} - u_Q) &= \xi_{O_1|\hat{k}_N} (u_{O_1} - u_Q) + \xi_{\hat{k}_N|O_1} (u_{\hat{k}_N} - u_Q) \\ \lambda_{g_{N,2}|\hat{k}_N}^{T_1} (u_{T_1} - u_Q) + \lambda_{g_{N,2}|\hat{k}_N}^{T_3} (u_{T_3} - u_Q) &= 3g_N^{r_N,2} |S_{\hat{k}, g_{N,2}}| + 3\xi_{\hat{k}_N|g_{N,2}} (u_{\hat{k}_N} - u_Q) \\ \lambda_{O_3|\hat{k}_N}^{T_1} (u_{T_1} - u_Q) + \lambda_{O_3|\hat{k}_N}^{T_2} (u_{T_2} - u_Q) &= \xi_{O_3|\hat{k}_N} (u_{O_3} - u_Q) + \xi_{\hat{k}_N|O_3} (u_{\hat{k}_N} - u_Q) \end{aligned}, \quad (64)$$

where the $\lambda_{g_{N,r_N}|\hat{k}_N}^{T_j}$ constants are calculated just like defined in eq. (48) and $\xi_{B|A}^{T_i}$ is set to zero (for it is nonexistent).

After some algebraic manipulation of equations (64), one can write the expression of the flux $\vec{\mathcal{F}}_{\hat{k}|r_N} \cdot \vec{N}_{T_j}$ only as a function of cell centered unknowns, yielding:

$$\vec{\mathcal{F}}_{\hat{k}|r_N} \cdot \vec{N}_{T_j} = - \begin{bmatrix} \eta_{\hat{k}_N|O_1} & \eta_{\hat{k}_N|O_2} & \eta_{\hat{k}_N|O_3} \end{bmatrix} \frac{A}{\sigma_{\hat{k}}} \begin{bmatrix} \xi_{O_1|\hat{k}_N} (u_{O_1} - u_Q) \\ 3g_N^{r_N,2} |S_{\hat{k}_N, g_{N,2}}| \\ \xi_{O_3|\hat{k}_N} (u_{O_3} - u_Q) \end{bmatrix} + \begin{bmatrix} \xi_{\hat{k}_N|O_1} \\ \xi_{\hat{k}_N|g_{N,2}} \\ \xi_{\hat{k}_N|O_3} \end{bmatrix} (u_{\hat{k}_N} - u_Q) \quad (65)$$

Separating the terms that are multiplied by $g_N^{g_{N,2}} \left| S_{\hat{k}_N, g_{N,2}} \right|$ and rearranging only for the \hat{k}_N terms in eq. (65) gives:

$$u_Q = \frac{1}{\sum_{\hat{k}} (\zeta_{\hat{k}} - \delta_{\hat{k}})} \left[\sum_{\hat{k}_N} \sum_{r_N} 3 \left(1 + \varepsilon_{r_N}^{\hat{k}_N} - \phi_{r_N|\hat{k}_N} \right) g_{N,r_N}^{\hat{k}_N} \left| S_{\hat{k}_N, r_N} \right| + \sum_{\hat{k}} (\zeta_{\hat{k}} - \delta_{\hat{k}}) u_{\hat{k}} \right], \quad (66)$$

with:

$$\varepsilon_{r_N}^{\hat{k}_N} = \frac{1}{\sigma_{\hat{k}_N}} \sum_{j=r_N}^{r_N+1} \lambda_{O_{r_N-1}|\hat{k}_N}^{T_{j-1}} \lambda_{O_{r_N+1}|\hat{k}_N}^{T_j} \eta_{O_{j+1}|\hat{k}_N}, \quad \phi_{r_N|\hat{k}_N} = \frac{\lambda_{O_{r_N-1}|\hat{k}_N}^{T_{r_N+1}} \lambda_{O_{r_N+1}|\hat{k}_N}^{T_{r_N-1}} \eta_{r_N|\hat{k}_N}}{\sigma_{\hat{k}_N}} \quad (67)$$

$$\begin{aligned} \phi_{O_j|\hat{k}_N} &= \begin{cases} \frac{\lambda_{O_{j,1}|O_j}^{T_{j+1}} \lambda_{O_{j,2}|O_j}^{T_{j+2}}}{\sigma_{O_j}} \eta_{O_j|\hat{k}_N} \xi_{\hat{k}_N|O_j} &, \\ 0 \text{ if } r = r_N & \end{cases}, \quad \phi_{\hat{k}_N|O_j} = \begin{cases} \frac{\lambda_{O_{j+1}|\hat{k}_N}^{T_{j+2}} \lambda_{O_{j+2}|\hat{k}_N}^{T_{j+1}}}{\sigma_{\hat{k}_N}} \eta_{\hat{k}_N|O_j} \xi_{\hat{k}_N|g_{N,j}} &, \\ \frac{\lambda_{g_{N,j+1}|\hat{k}_N}^{T_{j+2}} \lambda_{O_{j+2}|\hat{k}_N}^{T_{j+1}}}{\sigma_{\hat{k}_N}} \eta_{\hat{k}_N|O_j} \xi_{\hat{k}_N|g_{N,j}} & \end{cases} \\ \psi_{O_j|O_{j,i}} &= \begin{cases} \frac{\lambda_{O_{j,i}|O_j}^{T_{j+i}} \lambda_{O_{j,i+1}|O_j}^{I_j}}{\sigma_{O_j}} \eta_{O_j|O_{j,i}} \xi_{\hat{k}_N|O_j} &, \\ 0 \text{ if } r = r_N & \end{cases}, \quad \psi_{O_i|O_j} = \begin{cases} \frac{\lambda_{O_i|\hat{k}_N}^{T_{2(j+i)}} \lambda_{O_{i+1}|\hat{k}_N}^{T_j}}{\sigma_{\hat{k}_N}} \eta_{\hat{k}_N|O_i} \xi_{\hat{k}_N|g_{N,j}} &, \\ \frac{\lambda_{O_i}^{T_{2(j+i)}} \lambda_{g_{N,i+1}|\hat{k}_N}^{T_j}}{\sigma_{\hat{k}_N}} \eta_{\hat{k}_N|O_i} \xi_{\hat{k}_N|g_{N,j}} & \end{cases} \end{aligned} \quad (68)$$

4. Numerical Results

In order to evaluate the accuracy and robustness of our 3-D MPFA-D method, we present four test cases. In the first one, we solve a 3-D variation of the oblique drain case which was originally devised in [6] for 2-D domains and show that our method reproduces a linear solution exactly for the LPEW3 interpolation, even for heterogeneous and anisotropic media. In the second one [8], we consider a mildly anisotropic and homogeneous media and show the convergence rates of our method for the scalar variable and gradients considering different interpolation strategies. Not only we compare the MPFA-D scheme with other schemes but also we compare our interpolation method LPEW3 to the other interpolations. In the third problem [8], we evaluate the convergence rates of our formulation for the scalar variable and gradients for a highly heterogeneous and anisotropic media considering the LPEW3 interpolation and compared with the other interpolations considered. In the last problem, adapted from [42], we consider a strongly discontinuous and anisotropic diffusion tensor in order to evaluate the performance of our formulation with the different interpolation strategies, particularly to evaluate the limits of the method to produce solutions satisfying the Discrete Maximum Principle.

Following [8], we define the l^2 norms of the errors for the scalar unknown u and for the gradients ∇u . Hence, considering that the exact solution is given by u and the approximate solution is given by \hat{u} , we define the norms:

$$l_{rel,u}^2 = \left(\frac{\int_{\Omega} (u - \hat{u})^2}{\int_{\Omega} u^2} \right)^{1/2} = \left(\frac{\sum_i^{n_{vols}} (u - \hat{u})_i^2 |V_i|}{\sum_i^{n_{vols}} u_i^2 |V_i|} \right)^{1/2}, \quad (69)$$

$$l_{rel,\nabla u}^2 = \left(\frac{\int_{\Omega} \nabla(u - \hat{u})^2}{\int_{\Omega} \nabla u^2} \right)^{1/2} = \left(\frac{\sum_i^{n_{vols}} (\nabla u - \nabla \hat{u})_i^2 |V_i|}{\sum_i^{n_{vols}} (\nabla u)_i^2 |V_i|} \right)^{1/2}, \quad (70)$$

where the asymptotic convergence rate is given by [8]:

$$q = -3 \left(\frac{\log \frac{l_{\alpha_i}^2}{l_{\alpha_{i-1}}^2}}{\log \frac{N_i}{N_{i-1}}} \right), \quad (71)$$

for $i > 1$ and $\alpha = u$, ∇u and N is the total degrees of freedom (*dof*) of mesh i . Along with the convergence and performance evaluation, we provide the non-zero entries of our matrices (nmat).

The tests and methods. Examples 4.2 and 4.3 were run with the original meshes from [8]. All other meshes were generated based on the problems description. For comparison purposes, we have implemented different interpolation methods: the Inverse Distance Weighting (IDW) method and the Least-Squares Weighting (LSW) method found in [5, 31], respectively. It is important to mention that neither the LSW nor the IDW interpolation methods satisfy the LPC. In general, they do not guarantee exact solutions for some linear problems [5]. Furthermore, we also compare our results with the results of other methods presented in [8].

4.1. Linearity-Preserving Test: The adapted 3-D Oblique Drain Case

Here, we take the Test 6 from [6], originally devised for 2-D domains, and extend for 3-D domains. This problem consists in a heterogeneous and anisotropic media with $\Omega = [0, 1]^3$, which is splitted into three subdomains, representing, for instance, an oblique drain in porous media.

$$\begin{aligned}\Omega_1 &= \{(x, y) \in \Omega | \phi_1(x, y) < 0\}, \\ \Omega_2 &= \{(x, y) \in \Omega | \phi_1(x, y) > 0, \quad \phi_2(x, y) < 0\}, \\ \Omega_3 &= \{(x, y) \in \Omega | \phi_1(x, y) > 0\}.\end{aligned}$$

with $\phi_1(x, y) = y - \delta(x - 0.5) - 0.475$ and $\phi_2(x, y) = \phi_1(x, y) - 0.05$ and the slope of the drain is $\delta = 0.2$.

The problem was originally designed in such a way that its analytical solution is linear throughout $\Omega_1 \cup \Omega_2 \cup \Omega_3$ and is given by the following equation:

$$u(x, y) = -x - \delta y,$$

for which the source term is given by:

$$\mathcal{Q}(x, y) = \nabla \cdot [-\mathcal{K}(\vec{x})u].$$

The diffusion tensor is given by:

$$\mathcal{K}(\vec{x}) = R_z(\theta) \begin{pmatrix} \alpha & 0 & 0 \\ 0 & \beta & 0 \\ 0 & 0 & 1 \end{pmatrix} R_z(\theta)^T,$$

with $\theta = \arctan(\delta)$ and $R_z(\theta)$ is the rotation matrix in the z axis, defined as:

$$R_z(\theta) = \begin{pmatrix} \cos(\theta) & -\sin(\theta) & 0 \\ \sin(\theta) & \cos(\theta) & 0 \\ 0 & 0 & 1 \end{pmatrix}.$$

α and β are defined as:

$$\begin{pmatrix} \alpha \\ \beta \end{pmatrix} = \begin{pmatrix} 10^2 \\ 10 \end{pmatrix} \quad \text{on } \Omega_2, \quad \begin{pmatrix} \alpha \\ \beta \end{pmatrix} = \begin{pmatrix} 1 \\ 10^{-1} \end{pmatrix} \quad \text{on } \Omega_1 \cup \Omega_3.$$

For this problem, boundary conditions are given by:

$$g_D(x, y) = -x - \delta y \quad \text{on} \quad \Gamma_D, \quad g_N = 0 \quad \text{on} \quad \Gamma_N,$$

with Γ_D set at planes $x = 0, x = 1, y = 0, y = 1$ whereas Γ_N is set at the planes in $z = 0$ and $z = 1$.

Two different meshes were used to evaluate the performance of our scheme: the first containing only 15 dof and that does not require interpolation (since all its vertices are located at the boundary $\delta\Omega = \Gamma_D$) and the latter, a much finer mesh containing 46,923 dof. We use the LPEW3 interpolation for the inner vertices. Table 1 summarizes the norm of the error evaluated for the scalar property u . As expected, for both meshes, we obtained the exact solution to machine precision. Figures 5a and 5b show the color map and isosurfaces, respectively, for the solution obtained using the finest mesh from the test cases.

Table 1: Results for the Oblique Drain test.

dof	nmat	$l_{rel,u}^2$
15	47	1.62E-14
46,923	3,236,095	4.02E-15

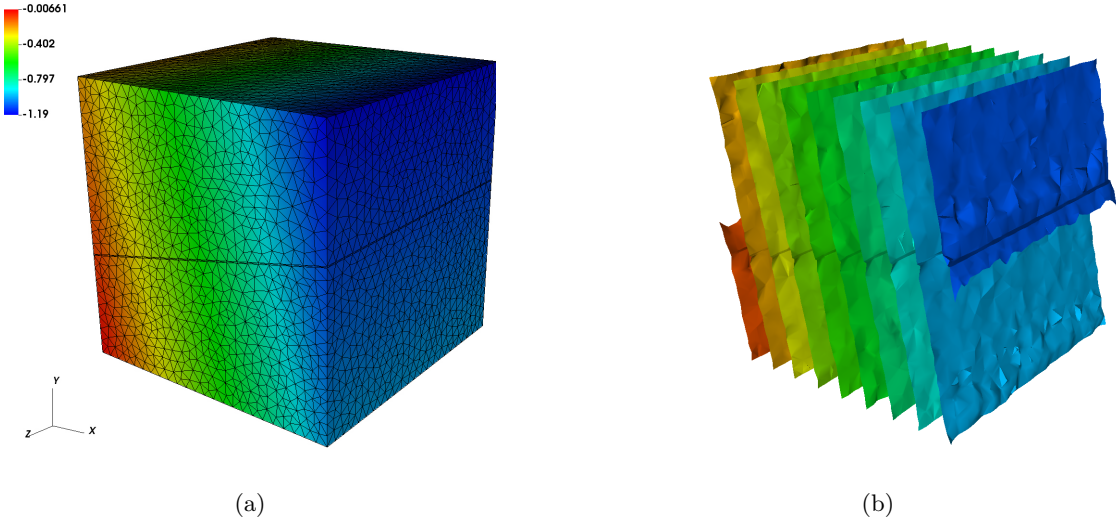


Figure 5: The Oblique Drain test. Results for the diffusive property u using the LPEW3 interpolation method. 5a shows the piecewise solution and 5b shows the isosurface contours. Mesh size: 46,923 volumes.

In table 2, we show comparative results using different interpolation strategies for meshes in which the volumes on Ω_2 are formed by skewed tetrahedra, due to its thin thickness. The results obtained show that both the IDW and the LSW were outperformed by the LPEW3 interpolation, since they do not satisfy the LPC.

Table 2: Results for the Oblique Drain test on a highly skewed mesh.

dof	$l_{rel,u}^2$		
	LSW	IDW	LPEW3
527	1.23E-02	2.36E-02	1.55E-14
2,151	1.17E-03	5.76E-03	1.28E-14

4.2. Mildly Anisotropic and Homogeneous Media

We consider the Benchmark Test Case 1 from [8] with a regular solution over the domain $\Omega = [0, 1]^3$, that implies in a non-homogeneous Dirichlet boundary condition Γ_D :

$$\mathbf{u}(x, y, z) = 1 + \sin(\pi x) \sin\left(\pi\left(y + \frac{1}{2}\right)\right) \sin\left(\pi\left(z + \frac{1}{3}\right)\right),$$

with $\mathcal{Q}(x, y) = -[\mathcal{K}] \nabla u$ and an anisotropic diffusion tensor:

$$[\mathcal{K}] = \begin{pmatrix} 1 & 0.5 & 0 \\ 0.5 & 1 & 0.5 \\ 0 & 0.5 & 1 \end{pmatrix}.$$

For comparison purposes, we present the results for this test case using the Linear-Preserving Scheme with Least Squares interpolation method (LPS-LS), introduced in [18]. We also present the results from different methods: Compact Discontinuous Galerkin 2 (CDG2) [43] and the Multipoint Flux Approximation O-method (MPFA-O) [2], both submitted to the Finite Volume for Complex Applications (FVCA) benchmark [8].

In tables 3, 4 and 5, we present the results for our method with the LPEW3, IDW and LSW interpolations. From these results, we can see that our method presents second order accuracy. The results show that our interpolation method has outperformed the IDW interpolation in terms of accuracy. Further analysis show that the IDW interpolation even fails to converge as the mesh is refined. On the other hand, regarding the LSW interpolation, the LPEW3 did not show much difference for the results obtained. The error obtained was only slightly better comparing both interpolations.

In figure 6 the MPFA-O method performs equally to our LPEW3, although the results in [8] show that the MPFA-O violates the DMP for tetrahedral meshes on both, the finest and the coarsest meshes. It is important to remember that the MPFA-O has regions where the scalar variable is extrapolated while the MPFA-D has full support for the scalar variable [3]. In figure 7, we show the $l_{rel, \nabla u}^2$ norm for all the tested interpolations and the other methods, showing that our method has first order convergence rate for fluxes. Figures 8 and 9 show the color map and the solution contours of the scalar variable u for the solutions obtained using the LPEW3 in different meshes.

Table 3: Results for the Mildly Anisotropic and Homogeneous Media problem using the LPEW3 interpolation method.

<i>dof</i>	nmat	u_{min}	u_{max}	$l_{rel, u}^2$	q_u	$l_{rel, \nabla u}^2$	$q_{\nabla u}$
44	172	0.392	1.633	1.338E-01	--	0.821	--
215	6,895	0.151	1.823	5.478E-02	1.689	0.600	0.593
2,003	107,331	0.036	1.969	1.411E-02	1.823	0.270	1.073
3,898	227,618	0.024	1.969	8.939E-03	2.057	0.207	1.195
7,711	476,645	0.024	1.978	5.557E-03	2.090	0.164	1.027
15,266	994,892	0.013	1.988	3.786E-03	1.686	0.129	1.048
30,480	2,072,944	0.007	1.994	2.289E-03	2.182	0.101	1.053
61,052	4,292,072	0.004	1.994	1.524E-03	1.758	0.079	1.071

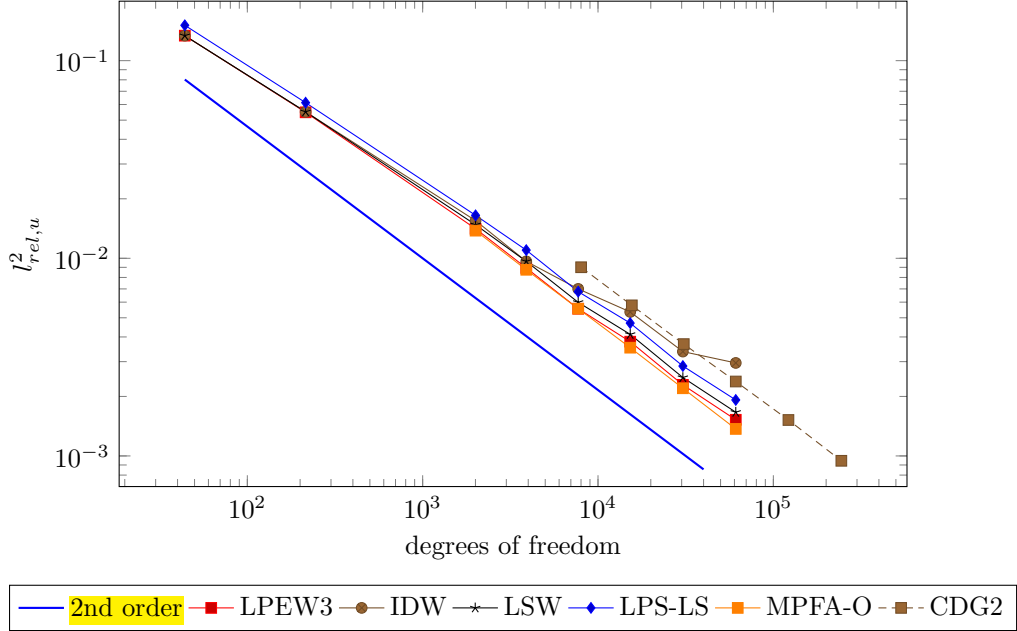


Figure 6: **Mildly Anisotropic and Homogeneous Media:** Results for the scalar variable u obtained using the LPEW3 interpolation method compared to other methods.

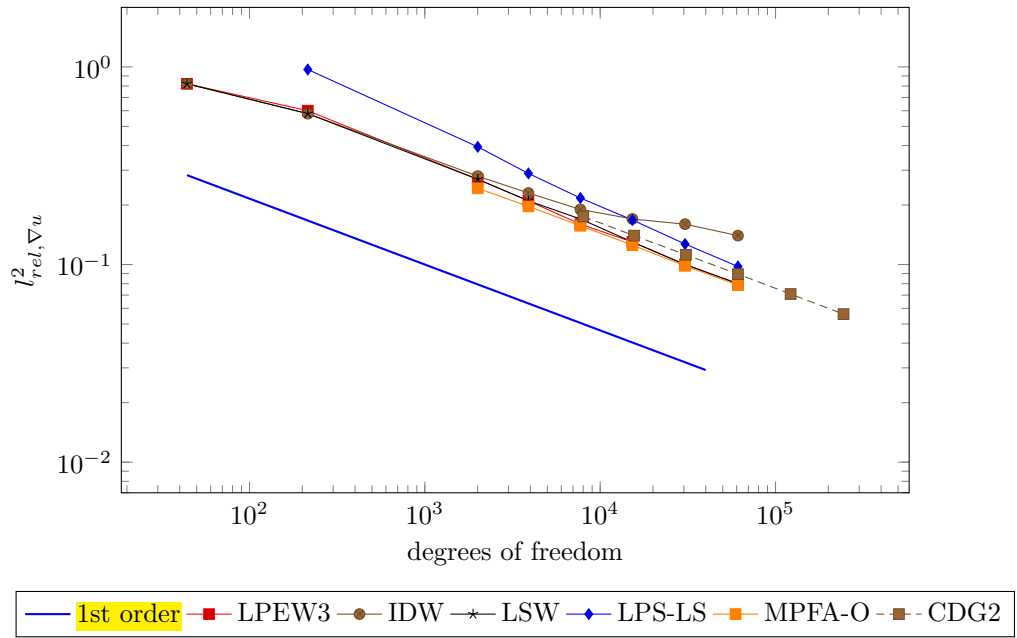


Figure 7: **Mildly Anisotropic and Homogeneous Media:** Results for the gradient of the scalar variable u obtained using the LPEW3 interpolation method compared to other methods.

Table 4: Results for the Mildly Anisotropic and Homogeneous Media problem using the IDW interpolation method.

<i>dof</i>	nmat	u_{min}	u_{max}	$l_{rel,u}^2$	q_u	$l_{rel,\nabla u}^2$	$q_{\nabla u}$
44	172	0.392	1.633	1.338E-01	--	0.821	--
215	6,895	0.153	1.819	5.509E-02	1.678	0.580	0.656
2,003	107,331	0.037	1.964	1.551E-02	1.704	0.282	0.967
3,898	227,618	0.025	1.967	1.061E-02	1.711	0.229	0.954
7,711	476,645	0.024	1.977	7.002E-03	1.828	0.194	0.724
15,266	994,892	0.014	1.987	5.353E-03	1.179	0.172	0.514
30,480	2,072,944	0.007	1.993	3.373E-03	2.004	0.156	0.448
61,052	4,292,072	0.005	1.994	2.955E-03	0.571	0.142	0.402

Table 5: Results for the Mildly Anisotropic and Homogeneous Media problem using the LSW interpolation method.

<i>dof</i>	nmat	u_{min}	u_{max}	$l_{rel,u}^2$	q_u	$l_{rel,\nabla u}^2$	$q_{\nabla u}$
44	172	0.392	1.633	1.338E-01	--	0.821	--
215	6,895	0.153	1.820	5.512E-02	1.677	0.583	0.646
2,003	107,331	0.037	1.968	1.478E-02	1.769	0.274	1.015
3,898	227,618	0.025	1.968	9.651E-03	1.920	0.212	1.158
7,711	476,645	0.024	1.978	5.987E-03	2.100	0.167	1.040
15,266	994,892	0.013	1.987	4.122E-03	1.640	0.132	1.045
30,480	2,072,944	0.007	1.994	2.493E-03	2.181	0.103	1.066
61,052	4,292,072	0.004	1.994	1.664E-03	1.747	0.081	1.063

4.3. Heterogeneous and Anisotropic Media

In this example, we consider the Benchmark Test Case 2 from [8] with a smoothly variable diffusion tensor that is given by:

$$\mathcal{K}(x, y, z) = \begin{pmatrix} y^2 + z^2 + 1 & -xy & -xz \\ -yx & x^2 + z^2 + 1 & -yz \\ -zx & -zy & x^2 + y^2 + 1 \end{pmatrix}$$

For a regular solution within the domain $\Omega = [0, 1]^3$ that implies in a non-homogeneous Dirichlet boundary condition on the whole boundary Γ_D :

$$u(x, y, z) = x^3 y^2 z + x \sin(2\pi xz) \sin(2\pi xy) \sin(2\pi z),$$

with $Q(x, y) = -\mathcal{K}\nabla u$.

We compare our interpolation, LPEW3, against the other interpolations IDW and LSW. Tables 6, 7 and 8 show the results obtained for the LPEW3, IDW and LSW interpolation methods, respectively. Figures 12 and 13 show the color map and the solution contours of the scalar variable using the LPEW3. From these results, we can clearly see that our interpolation method as well as the LSW interpolation method have 2nd order accuracy for the scalar variable and 1st order accuracy for the gradient (or fluxes). It is also important to mention that, in this case, the MPFA-D (with all 3 interpolations attempted) has produced a solution that satisfies the DMP, for the analytical solution to this problem is bounded by $u_{min} = -0.862$ and $u_{max} = -1.0487$.

4.4. Heterogeneous and Strongly Anisotropic Media.

This test is proposed by [42]. It consists of a full-tensor with large anisotropy ratio with principal axes orientation and jump in anisotropy ratio. We use the meshes provided in [8] as well. The diffusion tensor is defined, as:

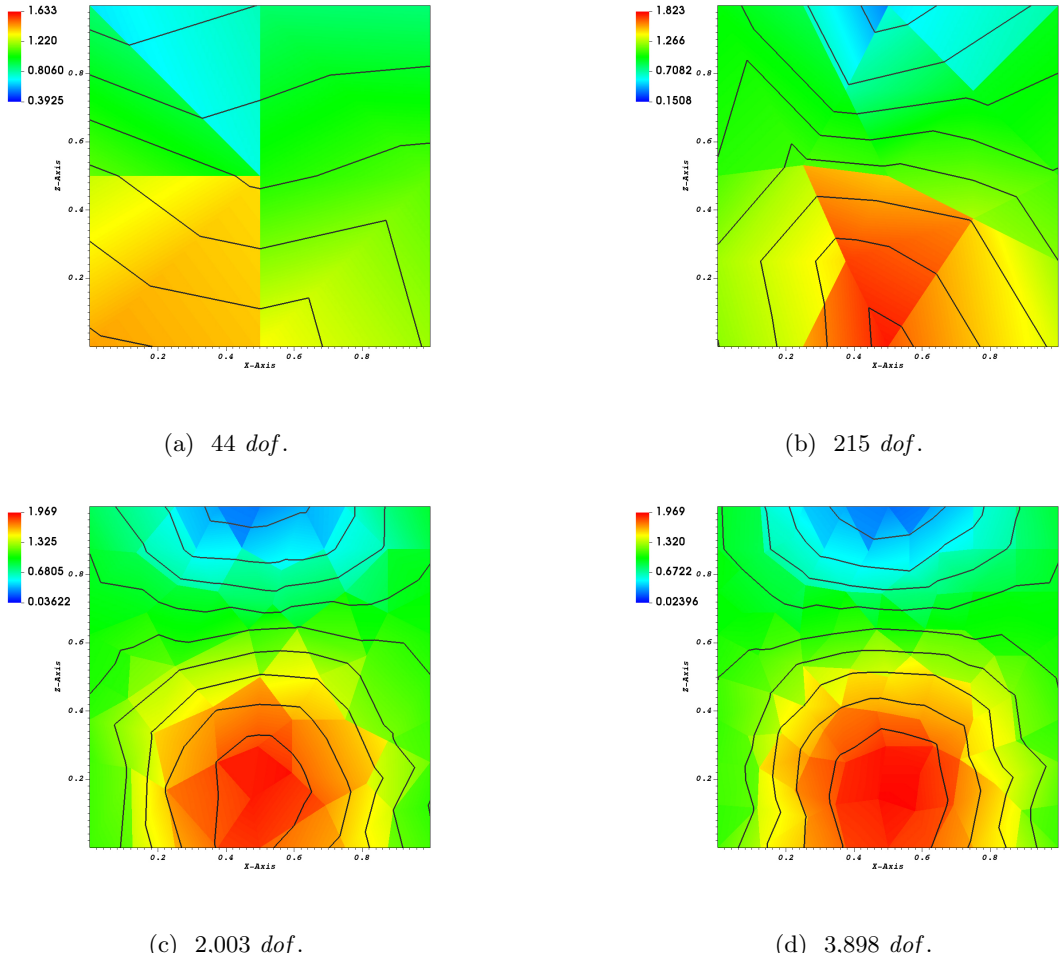


Figure 8: Color map and contours of the scalar variable u for the Mildly Anisotropic and Homogeneous Media problem. Slice for $y = 0$.

Table 6: Results for the Heterogeneous and Anisotropic Media using the LPEW3 interpolation method.

<i>dof</i>	nmat	u_{min}	u_{max}	$\ell^2_{rel,u}$	q_u	$\ell^2_{rel,\nabla u}$	$q_{\nabla u}$
44	172	-0.578	0.611	0.510	--	1.051	--
215	6,895	-0.447	0.990	0.506	0.015	0.980	0.132
2,003	107,331	-0.643	0.934	0.128	1.848	0.535	0.814
3,898	227,618	-0.681	0.933	0.083	1.945	0.448	0.802
7,711	476,645	-0.774	0.932	0.061	1.367	0.358	0.986
15,266	994,892	-0.809	0.975	0.038	2.105	0.283	1.028
30,480	2,072,944	-0.805	0.994	0.024	1.916	0.228	0.951
61,052	4,292,072	-0.831	1.031	0.017	1.654	0.180	1.004

$$\mathcal{K}(x, y, z) = \frac{1}{x^2 + y^2} \begin{pmatrix} \epsilon_x x^2 + \epsilon_y y^2 & (\epsilon_x - \epsilon_y)xy & 0 \\ (\epsilon_x - \epsilon_y)xy & \epsilon_y x^2 + \epsilon_x y^2 & 0 \\ 0 & 0 & \epsilon_z(z+1)(x^2 + y^2) \end{pmatrix},$$

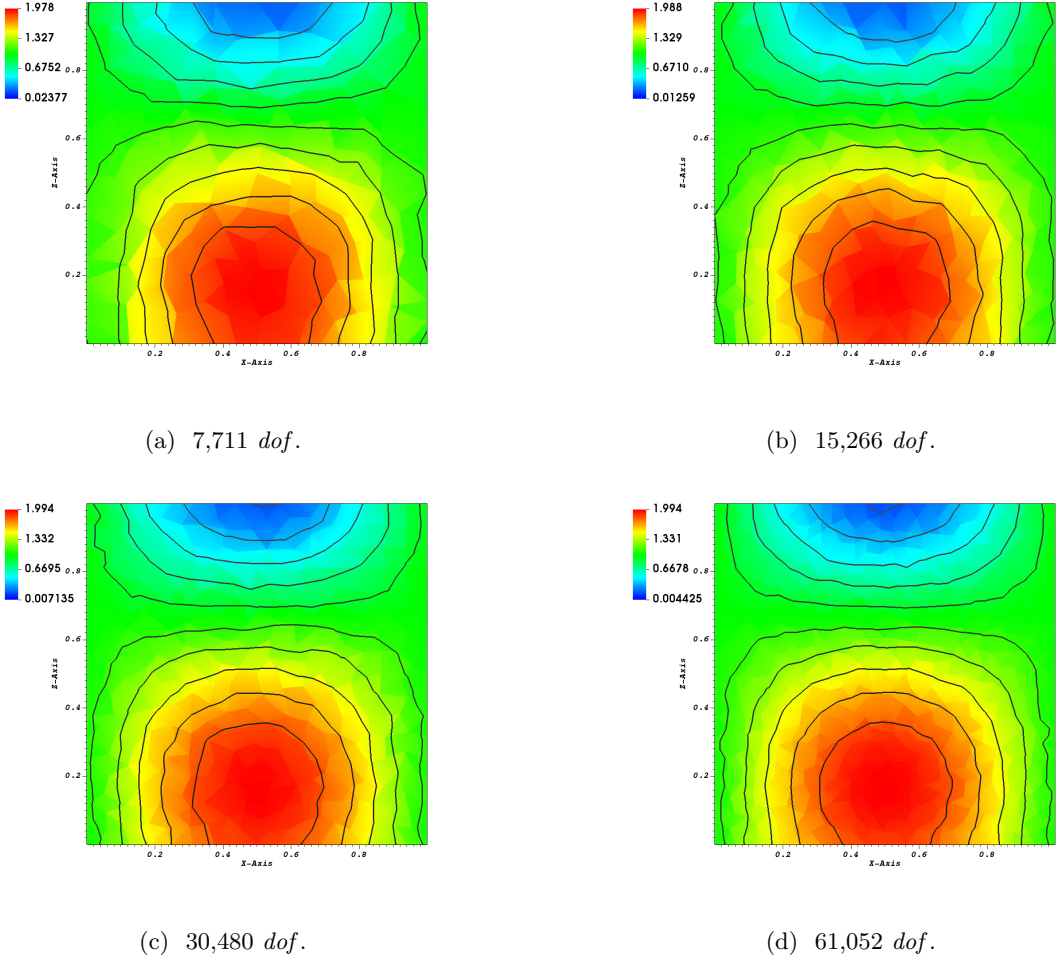


Figure 9: Color map and contours of the scalar variable u for the Mildly Anisotropic and Homogeneous Media problem (cont.). Slice for $y = 0$.

Table 7: Results for the Heterogeneous and Anisotropic Media using the IDW interpolation method.

dof	nmat	u_{min}	u_{max}	$l^2_{rel,u}$	q_u	$l^2_{rel,\nabla u}$	$q_{\nabla u}$
44	172	-0.578	0.611	0.510	--	1.051	--
215	6,895	-0.447	0.982	0.511	-0.004	0.988	0.117
2003	107,331	-0.635	0.925	0.136	1.780	0.556	0.773
3898	227,618	-0.668	0.932	0.090	1.848	0.464	0.810
7711	476,645	-0.770	0.928	0.069	1.181	0.378	0.901
15266	994,892	-0.805	0.972	0.046	1.775	0.312	0.854
30480	2,072,944	-0.802	0.992	0.033	1.482	0.259	0.805
61052	4,292,072	-0.827	1.031	0.025	1.200	0.218	0.735

where $\epsilon_x = 1$ and $\epsilon_z = 10$. We choose different values for ϵ_y in our tests. This problem is proposed such that:

$$u(x, y, z) = \sin(2\pi x)\sin(2\pi y)\sin(2\pi z), \quad (72)$$

and Dirichlet boundary conditions are applied on the whole boundary Γ_D , with $\mathcal{Q}(x, y) = -\mathcal{K}\nabla u$.

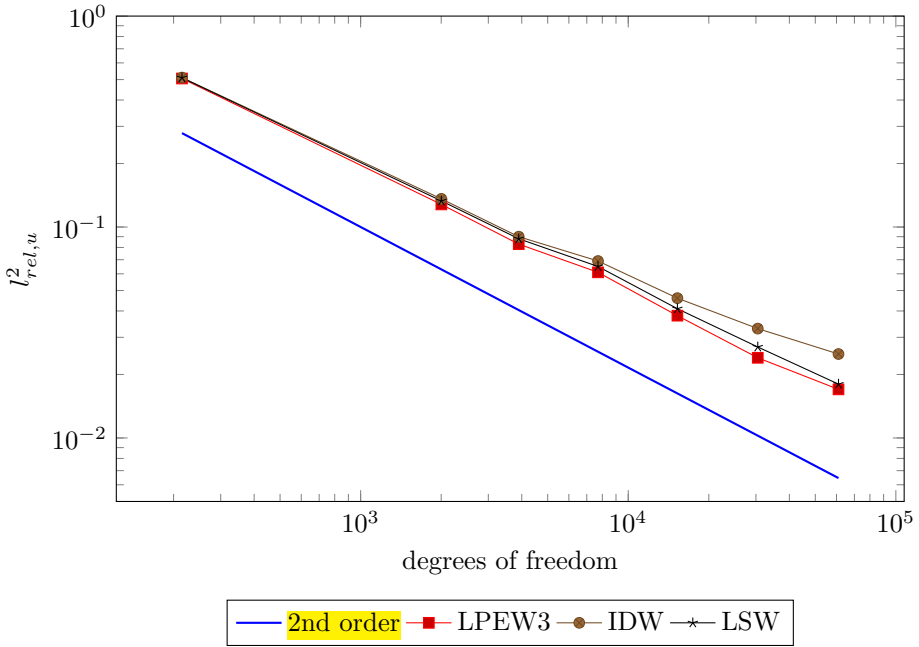


Figure 10: **Heterogeneous and Anisotropic Media.** Results for the scalar variable u obtained using the LPEW3 interpolation method compared to other interpolations.

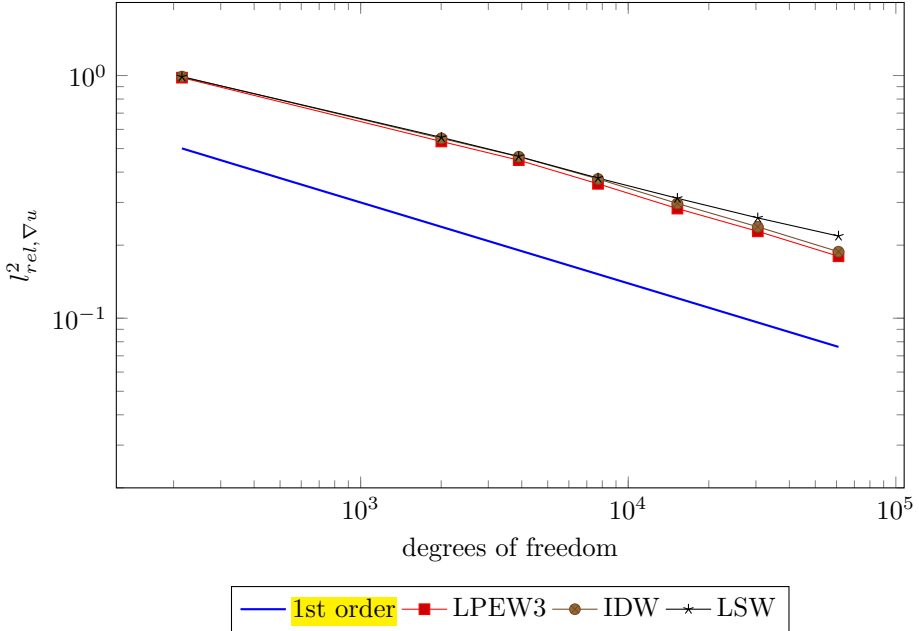


Figure 11: **Heterogeneous and Anisotropic Media.** Results for the gradient of the scalar variable u obtained using the LPEW3 interpolation method compared to other interpolations.

Our results show that, in the presence of strong anisotropy, the MPFA-D method coupled with the LPEW3 interpolation fails. Even though the LPEW3 interpolation satisfies the LPC, it does not guarantee the DMP nor even monotonicity [18]. Figures 14 and 15 show the results obtained for the MPFA-D with the LPEW3 and the other interpolation methods, respectively. It is important to mention that the findings in

Table 8: Results for the Heterogeneous and Anisotropic Media using the LSW interpolation method.

dof	nmat	u_{min}	u_{max}	$l^2_{rel,u}$	q_u	$l^2_{rel,\nabla u}$	$q_{\nabla u}$
44	172	-0.578	0.611	0.510	--	1.051	--
215	6,895	-0.446	0.984	0.510	0.000	0.990	0.113
2003	107,331	-0.639	0.928	0.133	1.804	0.551	0.787
3898	227,618	-0.676	0.932	0.088	1.892	0.463	0.784
7711	476,645	-0.772	0.930	0.065	1.292	0.375	0.931
15266	994,892	-0.806	0.974	0.041	2.021	0.297	1.023
30480	2,072,944	-0.806	0.995	0.027	1.856	0.238	0.967
61052	4,292,072	-0.832	1.031	0.018	1.689	0.188	1.001

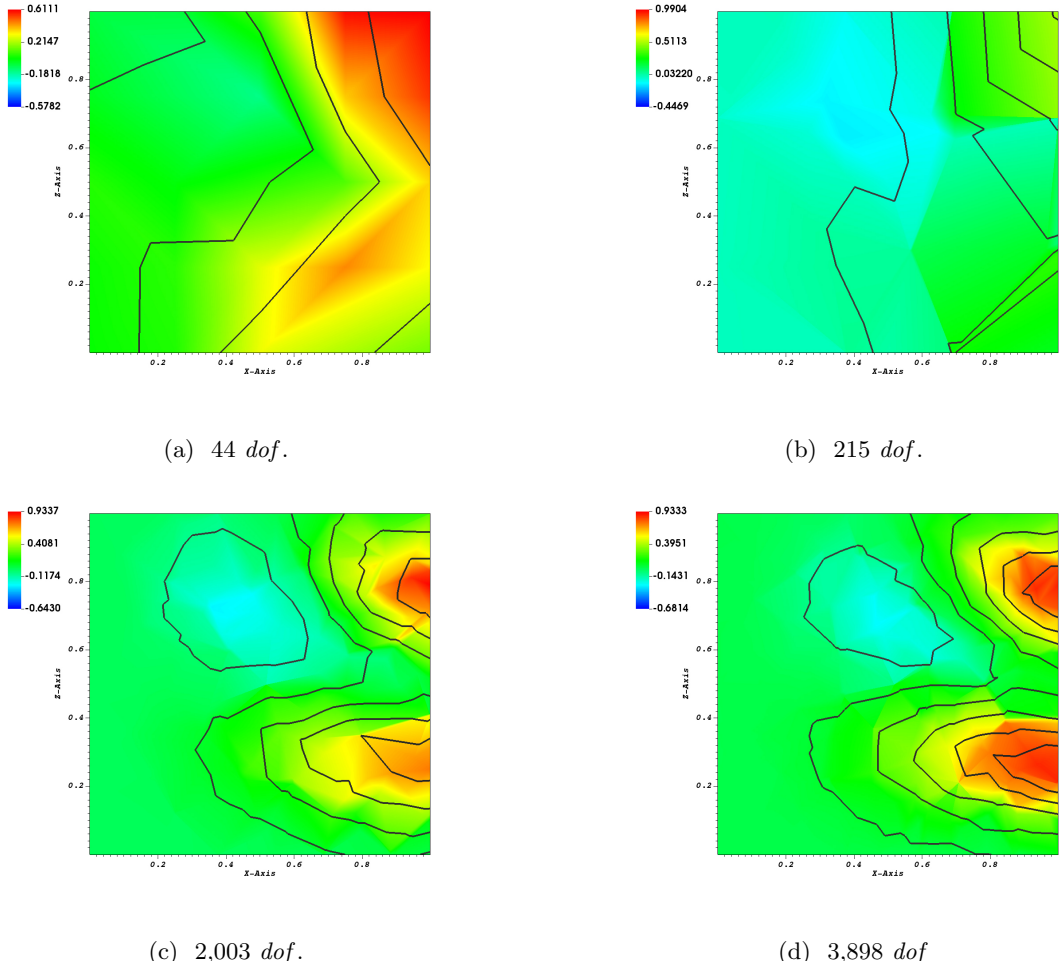


Figure 12: Color map and contours of the scalar variable u for the Heterogeneous and Anisotropic Media (cont.) Slice for $y = 0.25$.

[42] showed the same behavior for convergence presented in figure 14, using the same meshes from [8]. Figure 16 shows the color map and contours for $\epsilon_y = 10^{-3}$ with the LPEW3, LSW and the IDW interpolations and the analytical solution. Note that, in this case, both, LSW and IDW interpolations, clearly outperformed the LPEW3 interpolation. Further mesh refinement led to higher overshooting and undershooting of the

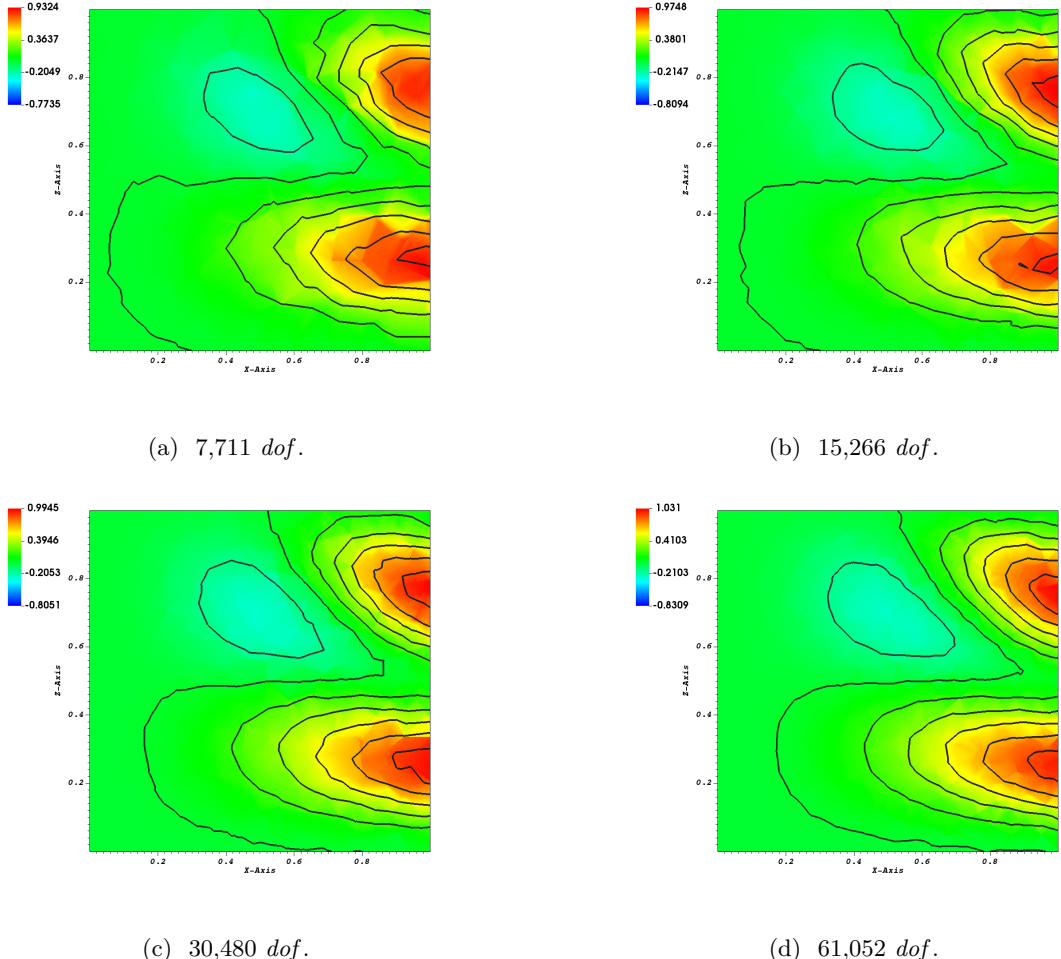


Figure 13: Color map and contours of the scalar variable u for the Heterogeneous and Anisotropic Media (cont.). Slice for $y = 0.25$.

LPEW3 interpolation whereas for the other interpolations, *i.e.*, IDW and LSW, results seemed to properly converge. In order to improve the performance of our interpolation method in such challenging cases, it would be necessary to use a non-linear finite volume method [19], or to develop some monotonicity fix, such as the one presented in [44].

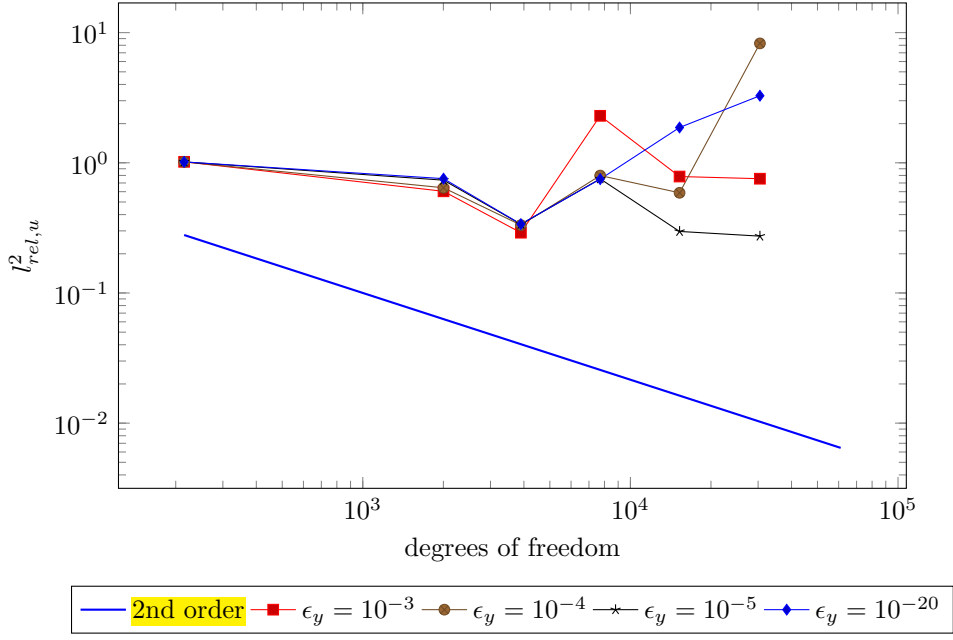


Figure 14: **Heterogeneous and Strongly Anisotropic Media.** Results for the scalar variable u obtained using the LPEW3 interpolation method and varying values of ϵ_y .

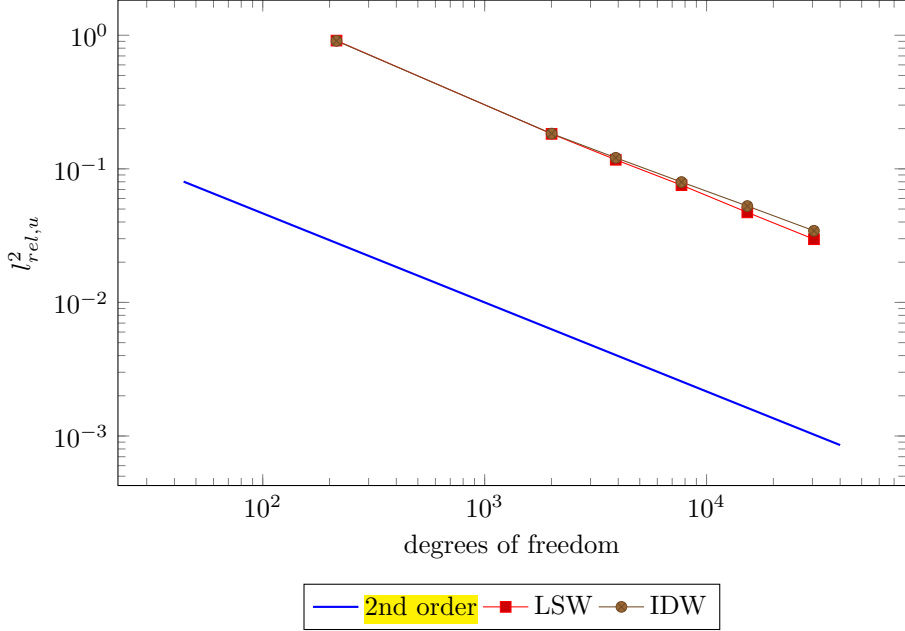


Figure 15: **Heterogeneous and Strongly Anisotropic Media.** Results for the scalar variable u obtained using the LSW and IDW interpolation methods for $\epsilon_y = 10^{-3}$.

5. Conclusions

In this paper, we have presented a 3-D formulation of a non-orthodox multipoint flux approximation finite volume scheme with a "Diamond" stencil (MPFA-D) for the solution of the steady-state diffusion problem in heterogeneous and anisotropic media, using tetrahedral meshes. Our new interpolation method (i.e., the

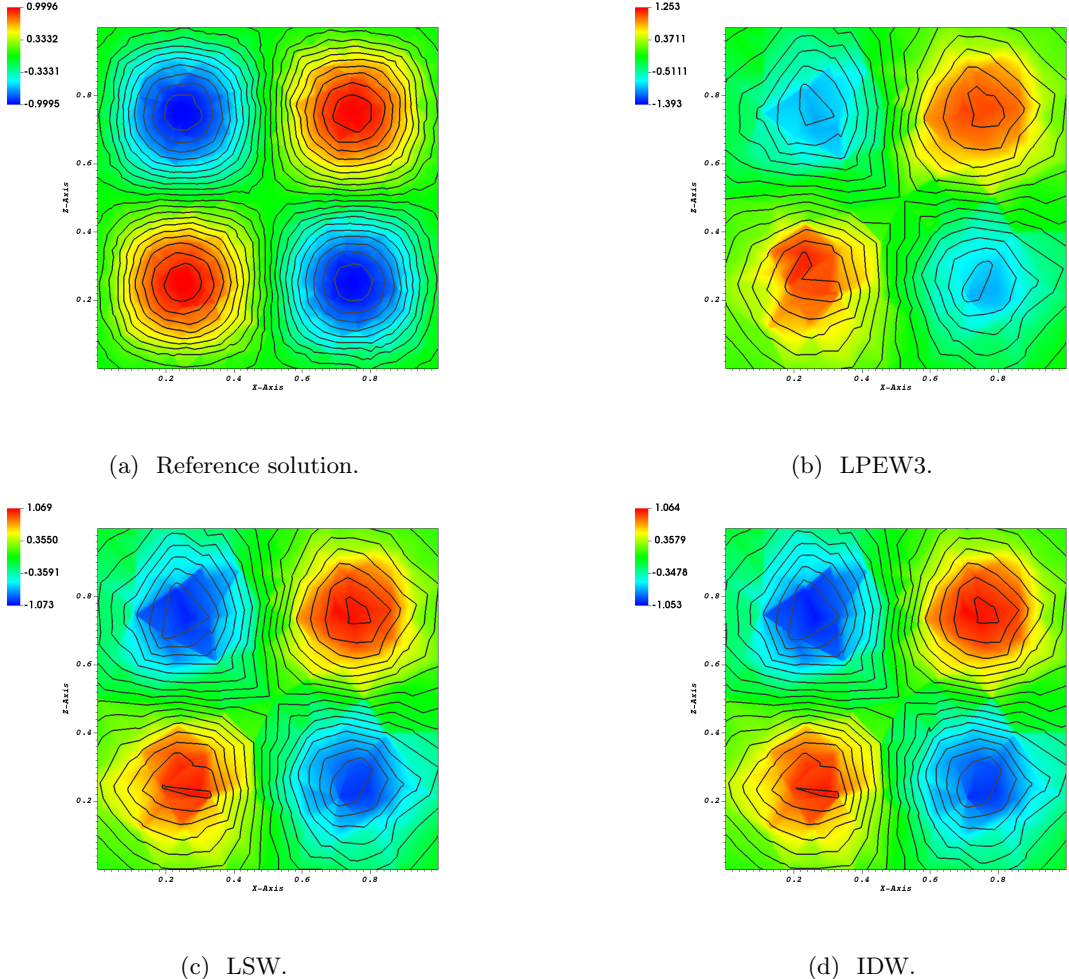


Figure 16: Color map and contours of the scalar variable u for the Heterogeneous and Strongly Anisotropic Media. Comparison for the three interpolation methods for a mesh size of 7,711 dof and using $\epsilon_y = 10^{-3}$. Slice for $y = 0.25$.

LPEW3) is constructed under the Linearity-Preserving Criterion (LPC), and it has presented second order accuracy for the scalar field and first order accuracy for gradients (or fluxes) for the majority of test cases attempted. In example 4.1 we have shown that the LPEW3 produces piecewise linear solutions even for highly skewed meshes while other interpolations such as the IDW and the LSW have failed to do it. In examples 4.2 and 4.3 we have shown that our method is quite robust even for heterogeneous and anisotropic media and for general unstructured tetrahedral meshes. On the other hand, example 4.4 has highlighted some of the limitations of the LPEW3 interpolation for very strong heterogeneous and anisotropic media. In the near future, we intend to generalize the method for general polyhedral meshes, study new interpolation strategies and develop possible fixes in order to reinforce the DMP or, at least monotonicity.

Acknowledgements

The authors would like to thank the following Brazilian research agencies for their financial support: Fundação de Amparo Ciência e Tecnologia do Estado de Pernambuco (FACEPE), National Council for Scientific and Technological Development (CNPq), Coordenação de Aperfeiçoamento de Pessoal de Nível Superior (CAPES).

References

- [1] Z. Gao, J. Wu, A linearity-preserving cell-centered scheme for the heterogeneous and anisotropic diffusion equations on general meshes, International Journal for Numerical Methods in Fluids 67 (12) (2011) 2157–2183. arXiv:<https://onlinelibrary.wiley.com/doi/pdf/10.1002/fld.2496>. doi:[10.1002/fld.2496](https://onlinelibrary.wiley.com/doi/abs/10.1002/fld.2496)
- [2] I. Aavatsmark, An introduction to multipoint flux approximations for quadrilateral grids, Computational Geosciences 6 (3) (2002) 405–432. doi:[10.1023/A:1021291114475](https://doi.org/10.1023/A:1021291114475)
- [3] M. G. Edwards, H. Zheng, A quasi-positive family of continuous darcy-flux finite-volume schemes with full pressure support, Journal of Computational Physics 227 (22) (2008) 9333 – 9364. doi:<https://doi.org/10.1016/j.jcp.2008.05.028>
- [4] P. R. M. Lyra, R. C. F. Lima, C. S. C. Guimarães, D. K. E. Carvalho, An edge-based unstructured finite volume procedure for the numerical analysis of heat conduction applications, Journal of the Brazilian Society of Mechanical Sciences and Engineering 26 (2) (2004) 160–169. doi:[10.1590/s1678-58782004000200007](https://doi.org/10.1590/s1678-58782004000200007)
- [5] L. E. S. Queiroz, M. R. A. Souza, F. R. L. Contreras, P. R. M. Lyra, D. K. E. Carvalho, On the accuracy of a nonlinear finite volume method for the solution of diffusion problems using different interpolations strategies, International Journal for Numerical Methods in Fluids 74 (4) (2014) 270–291. arXiv:<https://onlinelibrary.wiley.com/doi/pdf/10.1002/fld.3850>. doi:[10.1002/fld.3850](https://onlinelibrary.wiley.com/doi/abs/10.1002/fld.3850)
- [6] R. Herbin, F. Hubert, Benchmark on discretization schemes for anisotropic diffusion problems in general grids, Benchmark On Discretization Schemes For Anisotropic Diffusion Problems On General Grids For Anisotropic Heterogeneous Diffusion Problems (2008) 659–692Cited By 1.
- [7] F. R. L. Contreras, S. M. R. A. Lyra, P. R. M., D. K. E. Carvalho, A cell-centered multipoint flux approximation method with a diamond stencil coupled with a higher order finite volume method for the simulation of oilwater displacements in heterogeneous and anisotropic petroleum reservoirs, Computers & Fluids 127 (2016) 1 – 16. doi:<https://doi.org/10.1016/j.compfluid.2015.11.013>
- [8] R. Eymard, G. Henry, R. Herbin, F. Hubert, R. Klofkorn, G. Manzini, 3d benchmark on discretization schemes for anisotropic diffusion problems on general grids, Proceedings of Finite Volume for complex applications VU 4 (06 2011).
- [9] F. R. L. Contreras, P. R. M. Lyra, D. K. E. Carvalho, A new multipoint flux approximation method with a quasi-local stencil (mpfa-ql) for the simulation of diffusion problems in anisotropic and heterogeneous media, Applied Mathematical Modelling 70 (2019) 659 – 676. doi:<https://doi.org/10.1016/j.apm.2019.01.033>
- [10] L. Chang, G. Yuan, Cell-centered finite volume methods with flexible stencils for diffusion equations on general nonconforming meshes, Computer Methods in Applied Mechanics and Engineering 198 (17) (2009) 1638 – 1646. doi:<https://doi.org/10.1016/j.cma.2009.01.023>
- [11] J. Breil, P.-H. Maire, A cell-centered diffusion scheme on two-dimensional unstructured meshes, Journal of Computational Physics 224 (2) (2007) 785 – 823. doi:<https://doi.org/10.1016/j.jcp.2006.10.025>
- [12] M. Shashkov, S. Steinberg, Solving diffusion equations with rough coefficients in rough grids, Journal of Computational Physics 129 (2) (1996) 383 – 405. doi:<https://doi.org/10.1006/jcph.1996.0257>
- [13] O. Burdakov, I. Kapyrin, Y. Vassilevski, Monotonicity recovering and accuracy preserving optimization methods for postprocessing finite element solutions, Journal of Computational Physics 231 (01 2011). doi:[10.1016/j.jcp.2011.12.041](https://doi.org/10.1016/j.jcp.2011.12.041)
- [14] M. J. Mlacnik, L. J. Durlofsky, Unstructured grid optimization for improved monotonicity of discrete solutions of elliptic equation with highly anisotropic coefficients, Journal of Computational Physics 216 (2006) 337–361. doi:[10.1016/j.jcp.2005.12.007](https://doi.org/10.1016/j.jcp.2005.12.007).
- [15] M. Souza, F. R. L. Contreras, P. R. M. Lyra, D. K. E. Carvalho, A higher-resolution flow-oriented scheme with an adaptive correction strategy for distorted meshes coupled with a robust mpfa-d method for the numerical simulation of two-phase flow in heterogeneous and anisotropic petroleum reservoirs, SPE Journal 23 (09 2018). doi:[10.2118/182677-PA](https://doi.org/10.2118/182677-PA)
- [16] D. K. E. Carvalho, R. B. Willmersdorf, P. R. M. Lyra, Some results on the accuracy of an edgebased finite volume formulation for the solution of elliptic problems in nonhomogeneous and nonisotropic media, International Journal for Numerical Methods in Fluids 61 (2009) 237 – 254. doi:[10.1002/fld.1948](https://doi.org/10.1002/fld.1948).
- [17] S. Su, Q. Dong, J. Wu, A decoupled and positivity-preserving discrete duality finite volume scheme for anisotropic diffusion problems on general polygonal meshes, Journal of Computational Physics 372 (2018) 773 – 798. doi:<https://doi.org/10.1016/j.jcp.2018.06.052>
- [18] Z. Gao, J. Wu, A second-order positivity-preserving finite volume scheme for diffusion equations on general meshes, SIAM Journal on Scientific Computing 37 (1) (2015) A420–A438. arXiv:<https://doi.org/10.1137/140972470>, doi:[10.1137/140972470](https://doi.org/10.1137/140972470)
- [19] X. Lai, Z. Sheng, G. Yuan, Monotone finite volume scheme for three dimensional diffusion equation on tetrahedral meshes, Communications in Computational Physics 21 (2017) 162–181. doi:[10.4208/cicp.220415.090516a](https://doi.org/10.4208/cicp.220415.090516a).

- [20] I. Avatsmark, E. Reiso, R. Teigland, Control-volume discretization method for quadrilateral grids with faults and local refinements, *Computational Geosciences* 5 (1) (2001) 1–23. doi:10.1023/A:1011601700328.
URL <https://doi.org/10.1023/A:1011601700328>
- [21] M. G. Edwards, Unstructured, control-volume distributed, full-tensor finite-volume schemes with flow based grids, *Computational Geosciences* 6 (3) (2002) 433–452. doi:10.1023/A:1021243231313.
URL <https://doi.org/10.1023/A:1021243231313>
- [22] R. Ahmed, M. G. Edwards, S. Lamine, B. A. Huisman, M. Pal, Three-dimensional control-volume distributed multi-point flux approximation coupled with a lower-dimensional surface fracture model, *Journal of Computational Physics* 303 (2015) 470 – 497.
URL <http://www.sciencedirect.com/science/article/pii/S0021999115006609>
- [23] K. Lipnikov, G. Manzini, M. Shashkov, Mimetic finite difference method, *Journal of Computational Physics* 257 (PB) (2014) 1163–1227, cited By 140. doi:10.1016/j.jcp.2013.07.031.
URL <https://www.scopus.com/inward/record.uri?eid=2-s2.0-84897832938&doi=10.1016%2fj.jcp.2013.07.031&partnerID=40&md5=1b5c13f31d5d1af5b45242cb8cf28cf6>
- [24] R. Eymard, R. Herbin, T. Gallouët, Discretization of heterogeneous and anisotropic diffusion problems on general nonconforming meshes SUSHI: a scheme using stabilization and hybrid interfaces, *IMA Journal of Numerical Analysis* 30 (4) (2009) 1009–1043. arXiv:<http://academic.oup.com/imajna/article-pdf/30/4/1009/2066690/drn084.pdf>, doi:10.1093/imajna/drn084.
URL <https://dx.doi.org/10.1093/imajna/drn084>
- [25] J. Droniou, R. Eymard, A mixed finite volume scheme for anisotropic diffusion problems on any grid, *Numerische Mathematik* 105 (1) (2006) 35–71. doi:10.1007/s00211-006-0034-1.
URL <https://doi.org/10.1007/s00211-006-0034-1>
- [26] B. Andreianov, F. Boyer, F. Hubert, Discrete duality finite volume schemes for leraylionsttype elliptic problems on general 2d meshes, *Numerical Methods for Partial Differential Equations* 23 (1) (2007) 145–195. arXiv:<https://onlinelibrary.wiley.com/doi/pdf/10.1002/num.20170>, doi:10.1002/num.20170.
URL <https://onlinelibrary.wiley.com/doi/abs/10.1002/num.20170>
- [27] F. Hermeline, A finite volume method for approximating 3d diffusion operators on general meshes, *Journal of Computational Physics* 228 (2009) 5763–5786. doi:10.1016/j.jcp.2009.05.002.
- [28] G. Yuan, Z. Sheng, Monotone finite volume schemes for diffusion equations on polygonal meshes, *Journal of Computational Physics* 227 (12) (2008) 6288 – 6312. doi:<https://doi.org/10.1016/j.jcp.2008.03.007>.
URL <http://www.sciencedirect.com/science/article/pii/S0021999108001587>
- [29] Z. Sheng, G. Yuan, A nine point scheme for the approximation of diffusion operators on distorted quadrilateral meshes, *SIAM Journal on Scientific Computing* 30 (3) (2008) 1341–1361. doi:10.1137/060665853.
- [30] D. Li, H. Shui, M. Tang, On the finite difference scheme of two-dimensional parabolic equation in a non-rectangular mesh, *J Numer Methods Comput Appl* 1 (4) (1980) 217–224, cited By 34.
- [31] Y. Coudière, J.-P. Vila, P. Villedieu, Convergence rate of a finite volume scheme for a two dimensional convection-diffusion problem, *ESAIM: Mathematical Modelling and Numerical Analysis - Modélisation Mathématique et Analyse Numérique* 33 (3) (1999) 493–516.
URL http://www.numdam.org/item/M2AN_1999__33_3_493_0
- [32] S. Wang, X. Hang, G. Yuan, A pyramid scheme for three-dimensional diffusion equations on polyhedral meshes, *Journal of Computational Physics* 350 (2017) 590 – 606. doi:<https://doi.org/10.1016/j.jcp.2017.08.060>.
URL <http://www.sciencedirect.com/science/article/pii/S0021999117306411>
- [33] J. Wu, Z. Gao, Interpolation-based second-order monotone finite volume schemes for anisotropic diffusion equations on general grids, *Journal of Computational Physics* 275 (2014) 569 – 588. doi:<https://doi.org/10.1016/j.jcp.2014.07.011>.
URL <http://www.sciencedirect.com/science/article/pii/S0021999114004914>
- [34] S. K. Verma, Flexible grids for reservoir simulation, Ph.D. thesis, Stanford University (1996).
- [35] D. Yang, Z. Gao, A linearity-preserving vertex interpolation algorithm for cell-centered finite volume approximations of anisotropic diffusion problems, *International Journal of Numerical Methods for Heat & Fluid Flow* ahead-of-print (2019) 237 – 254.
- [36] K. Lipnikov, M. Shashkov, D. Svyatskiy, Y. Vassilevski, Monotone finite volume schemes for diffusion equations on unstructured triangular and shape-regular polygonal meshes, *Journal of Computational Physics* 227 (2007) 492–512. doi:10.1016/j.jcp.2007.08.008.
- [37] T. L. Bergman, A. Lavine, F. P. Incropera, *Fundamentals of heat and mass transfer*, 2011.
- [38] J. Bear, *Dynamics of Fluids in Porous Media*, Dover Publications, 2013.
- [39] R. B. Bird, W. E. Stewart, E. N. Lightfoot, *Transport Phenomena*, 2007.
- [40] C. Hirsch, *Numerical computation of internal and external flows*, Elsevier/Butterworth-Heinemann, 2007.
- [41] J. W. Gibbs, E. B. Wilson, *Vector analysis; a text-book for the use of students of mathematics and physics*, 1958.
- [42] M. G. Edwards, H. Zheng, Quasi m-matrix multifamily continuous darcy-flux approximations with full pressure support on structured and unstructured grids in three dimensions, *SIAM Journal on Scientific Computing* 33 (2) (2011) 455–487.
- [43] R. Klöfkorn, Benchmark 3d: The compact discontinuous galerkin 2 scheme 4 (01 2011). doi:10.1007/978-3-642-20671-9_100.
- [44] D. Kuzmin, M. Shashkov, D. Svyatskiy, A constrained finite element method satisfying the discrete maximum principle for anisotropic diffusion problems, *Journal of Computational Physics* 228 (2009) 3448–3463.